Remote Sensing of Environment 216 (2018) 154–170

Contents lists available at ScienceDirect

Remote Sensing of Environment

journal homepage: www.elsevier.com/locate/rse

Remote sensing of water constituent concentrations using time series of in-situ hyperspectral measurements in the Wadden Sea

Behnaz Arabi[a,*], Mhd Suhyb Salama[a], Marcel Robert Wernand[b], Wouter Verhoef[a]

[a] Faculty of Geo-Information Science and Earth Observation (ITC), Department of Water Resources, University of Twente, P.O. Box 217, 7500AE Enschede, the Netherlands

[b] Department of Coastal Systems, Marine Optics and Remote Sensing, Royal Netherlands Institute for Sea Research (NIOZ), P.O. Box 59, 1790AB Den Burg, Texel, the Netherlands

ARTICLE INFO

Keywords:
Remote sensing
Turbid waters
The 2SeaColor model
Hyperspectral measurements
Tidal effect
Solar zenith angle
The NIOZ jetty station
The Wadden Sea

ABSTRACT

This study aimed to investigate the capability of the two-stream radiative transfer model 2SeaColor for the simultaneous retrieval of Chlorophyll-a (Chla), Suspended Particulate Matter (SPM) and Colored Dissolved Organic Matter (CDOM) concentrations from remote sensing measurements under various conditions (i.e., solar zenith angle values (SZAs) and water turbidity levels). For this evaluation, a time series of diurnal in-situ hyperspectral measurements of remote sensing reflectance (R_{rs}) concurrent with in-situ measured Chla and SPM concentrations between 2008 and 2010 by the NIOZ jetty station (the NJS), located in the Dutch part of the Wadden Sea, was used. Validation of the model retrievals against in-situ measurements showed an acceptable accuracy (Chla: $R^2 = 0.80$ and RMSE = 2.98 [mg m^{-3}]; SPM: $R^2 = 0.89$ and RMSE = 2.53 [g m^{-3}]) with good agreement between the temporal trends of measured and retrieved concentration values over multiple years. However, the model inversion results yielded less good estimates at SZA $> 60^{\circ}$ during winter. Furthermore, the effect of the tide on the variation of daily time series of Chla and SPM concentrations was analyzed. At the particular NJS location, the tidal effects on the concentrations of SPM and Chla were found to be small. The capability of the 2SeaColor model to retrieve reliable estimates, and the favorable location of the NJS, which is little influenced by tidal phase variations, contribute to a better understanding of the long-term variability of Chla and SPM concentrations. The results of this study may support the ongoing efforts on Sentinel-3 Ocean and Land Color Instrument (OLCI) calibration and validation at the Dutch Wadden Sea.

1. Introduction

Conservation of European coastal waters in a healthy environmental state has become a high priority as regulated in the "Marine Strategy Framework Directive, 2008/56/EC" (Mélin et al., 2011). One of the most important coastal ecosystems, which have drawn great attention in Europe, is the Wadden Sea. Conservation of this tidal ecosystem as the largest unbroken system of intertidal mudflats in the world, and as one of the 193 natural World Heritage properties, has become compulsory since July 2009 (Sijtsma et al., 2015). Accordingly, particular attention has been paid by the Netherlands, Denmark, and Germany to protect this area since the early years of the last century (Bashir, 2016). Maintaining this coastal area in a healthy state requires a continuous monitoring approach that can capture the dynamics of water constituent concentrations (Chla, SPM, and CDOM). Remote sensing is an efficient technique that provides information on water constituent concentrations (hereafter referred to as WCCs) on high spatio-temporal scales (Kirk, 1994; Philippart et al., 2013). In the Wadden Sea, remote sensing has often been applied to produce tidal flat maps (e.g., sediment types maps or finding locations with seagrass). For example, radar and laser data has been used to detect the land-water boundaries (Niedermeier et al., 2005; Wang, 1997; Wimmer et al., 2000). However, there are only a few studies available on remote sensing algorithms of optical properties that can be applied for continuous monitoring of WCCs in this area (Hommersom, 2010). Recent studies show that remote sensing of this complex coastal area seems both possible and beneficial. Nevertheless, ocean color products may comprise errors of up to 50% due to the following major problems (Arabi et al., 2016; Cadee and Hegeman, 2002; Hommersom et al., 2010; Philippart et al., 2013, 2010; Van der Woerd and Pasterkamp, 2008).

1.1. Atmospheric correction problem

Satellite images are widely used for remote sensing of WCCs in

* Corresponding author.
E-mail address: b.arabi@utwente.nl (B. Arabi).

https://doi.org/10.1016/j.rse.2018.06.040
Received 1 August 2017; Received in revised form 16 May 2018; Accepted 25 June 2018
Available online 11 July 2018
0034-4257/ © 2018 Elsevier Inc. All rights reserved.

coastal areas. However, performing an accurate atmospheric correction is a most challenging task which may cause significant errors especially in coastal waters studies (Salama et al., 2004; Wang, 2007; Wang et al., 2009, 2007; Wang and Gordon, 1994; Wang and Shi, 2007). One possible approach to minimize the problem of atmospheric effects on remote sensing of coastal waters is using ground-based water leaving reflectance measurements which are collected at the study site (Loisel et al., 2013; Salama et al., 2012; Wernand and Der Woerd, 2010). In the present study, we had the opportunity to work with a unique dataset of time series of diurnal in-situ hyperspectral water leaving reflectance concurrently with in-situ measured Chla and SPM concentrations collected on a regular basis (noon time) throughout multiple years at the NJS. By using this continuous in-situ dataset, the effect of the atmosphere on the remote sensing dataset could be minimized. Accordingly, it was feasible to have the best validation of the hydro-optical model using this dataset, which was collected over different seasons and conditions. On the other hand, eliminating the effect of the atmosphere as the most important source of models' retrieval errors makes it better possible to evaluate the contribution of other factors (e.g., water turbidity and SZAs) to the model's retrieval accuracy.

1.2. Hydro-optical models saturation in the presence of high turbidity

Most hydro-optical models are not capable enough to simulate water leaving reflectance values under the condition of high WCCs in turbid waters. Therefore, saturation occurs when modeling R_{rs} at high turbidity, and consequently retrieving WCCs from remote sensing measurements over turbid waters will often fail. For example, Gordon et al. (1988) developed a semi-analytical optical model which predicts the upwelling spectral radiance as a function of the phytoplankton pigment concentration at the sea surface level for open oceans. Based on Gordon's model, the variations in the phytoplankton backscattering and absorption, and the associated detrital material determine the radiance values variations. Lee et al. (2002) developed a multiband quasi-analytical algorithm based on Gordon's model to retrieve backscattering and absorption coefficients from remote sensing reflectance spectra for both open oceans and coastal waters. However, both the Gordon and Lee models suffer from early saturation at high turbidities (Salama and Shen, 2010). Fettweis et al. (2007) developed a semi-analytical algorithm to investigate the relationships between the backscattering coefficient, the absorption coefficient, water leaving reflectance and WCCs in the Belgian/Dutch coastal area. However, also their model was only appropriate for low turbidity waters. Since the Wadden Sea is considered a high turbidity coastal area (Hommersom, 2010), it is crucial to select a reliable hydro-optical model that does not saturate too soon for modeling of water leaving reflectance values under high water turbidity conditions. In this study, we implemented a new hydro-optical model which comprises an analytical forward model including an inversion scheme known as the 2SeaColor model (Salama and Verhoef, 2015) for the simultaneous retrieval of WCCs from in-situ hyperspectral measurements of remote sensing reflectance, R_{rs}. The 2SeaColor model was developed while maintaining a relative simplicity by applying the two-stream approach including direct sunlight, based on Duntley (1941). The model considers multiple scattering, which delays the saturation of water reflectance under high turbidity conditions. Most hydro-optical models consider only single scattering (Salama and Verhoef, 2015), and therefore saturate in producing R_{rs} values already at moderate turbidity conditions.

1.3. SZA effect on the accuracy of the hydro-optical models' retrievals

High SZA values can affect the quality of remote sensing data and accordingly the accuracy of WCC retrievals using different hydro-optical models. Geostationary satellites (e.g., Geostationary Ocean Color Imager (GOCI), which observes a region eight or more times a day) provide observations from the early morning to the late afternoon, and many data can be obtained under large SZA conditions (Chen, 2017). In addition, at the location of the Wadden Sea, high SZA variations can be found in winter around noon and in summer early in the morning or evening. Therefore, it is essential to use a hydro-optical model that includes the SZA effect when working with time series of optical measurements covering the whole year in this area. So far, a few studies have evaluated the effect of SZA on the accuracy of WCC retrievals using remote sensing measurements. For example, Volpe et al. (2007) assessed the uncertainties of Chla retrievals in the Mediterranean Sea using the OC4V4 algorithm and concluded that this algorithm was not capable enough to retrieve Chla concentration values at this region due to the weak light intensity. Chaves et al. (2015) assessed the ocean color products (e.g., Chla and spectral marine IOPs) from MODIS AQUA data in the Western Arctic Ocean. They found that the empirical algorithms were positively biased in comparison with in-situ measurements due to weak light and high latitudes. Li et al. (2017) investigated the performances of seven widely used Chla retrieval algorithms (i.e., OC2, OC3M, OC3V, OC4V4, Clark, ocean-color index, and Yellow Sea Large Marine Ecosystem Ocean Color Work Group) under high SZA conditions using the global in-situ ocean color dataset (NASA bio-optical marine algorithm dataset). The results showed that the performances of all seven algorithms decreased significantly under high SZA values compared with those under low to moderate SZA values. They later investigated the possibility of improving these models by adjusting the coefficients of the algorithms using the in-situ dataset under the condition of high SZA values. They showed that the results could not be significantly improved by adjusting the models for high SZA conditions. In this study, for the first time, we evaluated the effect of SZA on WCC retrievals using remote sensing measurements in the Wadden Sea. The 2SeaColor model includes incident direct sunlight while it computes the directional-hemispherical reflectance factor (DHRF) as a function of the SZA. Therefore the SZA effect on R_{rs} measurements is considered into this hydro-optical model while doing WCC retrievals (Salama and Verhoef, 2015), although no effects of the viewing zenith angle (VZA) are considered in this model. Consequently, by analyzing a time series of nearly continuous high quality in-situ hyperspectral measurements recorded over multiple years at the NJS, it was feasible to explore and test the model-based retrievals under various SZAs using the 2SeaColor model.

1.4. Reliability of local specific inherent optical properties (SIOPs)

One of the challenges associated with applying remote sensing techniques in coastal waters is that the SIOPs show high spatial and temporal variability in different coastal areas (Babin, 2003; Babin et al., 2003). These variations are due to numerous factors, including changes in the water source, sediment type, phytoplankton species composition and CDOM sources. Since the Wadden Sea is a vast coastal area with numerous sources of water inputs, it is crucial to evaluate the reliability of local SIOPs over the location and time in this region. (Salama and Su, 2010). However, for this area, detailed information about seasonal SIOPs is still lacking. For example, Babin et al. (2003) documated SIOPs estimates in the Wadden Sea, but they merged them with the North Sea SIOPs. However, the Wadden Sea SIOPs are different from those of the North Sea (Hommersom, 2010). In this study, we used a set of measured SIOPs, which have been collected by Hommersom et al. (2009) at 37 locations between 2006 and 2007 at the Wadden Sea. At the time when this study was conducted, these measured SIOPs were the only available ones as representative of water constituent characteristics in the Wadden Sea. However, some analysis was performed to ensure the reliability of these measured SIOPs to be implemented for the 2SeaColor parametrization during different seasons at the NJS.

1.5. Tidal variation

In remote sensing studies in coastal regions, tidal phase variations

might interfere with time series of optical measurements and consequently with retrieved WCCs using hydro-optical models. Many studies have been conducted to evaluate the effect of tide on retrieved WCCs from remote sensing observations in different coastal areas. For example, Eleveld et al. (2014) investigated the relationship between the tidal phase and retrieved SPM concentration values using MERIS images in the Western Scheldt located in the southwest of the Netherlands. They concluded that tide is one of the leading factors, affecting the variations in estimated surface SPM concentrations for this tidal area. He et al. (2013) generated hourly SPM concentration maps from GOCI observations. They showed that various regions had different diurnal variations concerning tidal phases in Hangzhou Bay. Wang et al. (2013) investigated the effect of the tide on the diurnal variation of ocean optical properties using GOCI images in the western Pacific region. Doxaran et al. (2009a, 2009b) used one-year time series of in-situ measurements to show the tidal phase effect on turbidity variations in the upper part of a micro-tidal estuary using Moderate-resolution Imaging Spectroradiometer (MODIS) images. Valente and da Silva (2009) investigated the effect of tide on water turbidity and circulation in the Tagus estuary using multi-sensor satellite observations. The Wadden Sea is also a tidal area, which is connected to the North Sea by a series of tidal inlets (Ridderinkhof et al., 1990). Like anywhere else, at the NJS location there is a daily shift of about 1 h in the tidal phase, so that all phases pass by in about one month. Thus, the tidal phase variation might interfere with the time series of measurements since the in-situ R_{rs} measurements concurrent with WCCs are taken around noon local time on all days. Therefore, the effect of tide needs to be considered carefully when interpreting time series of water quality products in this region. In this study, for the first time, we did a brief analysis to verify whether the time series analysis of WCCs at the NJS is affected by tidal phase variations. Although this assessment is not intended as an in-depth study of tidal effects, its conclusion plays a vital role in following the long-term temporal courses of WCCs at the NJS.

After mentioning the main problems of remote sensing of water quality at the Wadden Sea, we defined the main objectives of this study as evaluation and validation of the 2SeaColor model performance for WCC retrievals under different SZAs and water turbidity conditions at the NJS. Finally, we will discuss the application of this validated hydro-optical model to be implemented on the ground-based remote sensing measurements and satellite images.

2. Study area

The study area of this work is the Dutch Wadden Sea. This is the area located between the North Sea in the northwest and the mainland of the Netherlands in the southeast, and between the Eems-Dollard estuary in the northeast and the Marsdiep in the southwest (Ridderinkhof et al., 1990). This area is considered as a shallow, well-mixed tidal region with a surface area of 2500 km^2 and consists of several tidal basins (Ridderinkhof et al., 1990). The satellite image in Fig. 1 shows the south-western part of the Wadden Sea, with parts of the Dutch mainland on the right and the island of Texel at the bottom left, and Vlieland and Terschelling to the north. As this SPOT satellite image (spatial resolution 20 m) shows, the bottom can be seen in large parts of the Dutch Wadden Sea, illustrating clearly that the sea bottom effect can influence remote sensing of optical measurements in this shallow coastal area (Lee et al., 1999). However, this was not the case for the NJS data due to the moderate turbidity and the depth of the water (> 5 m) at that location, so that the bottom effect on measured reflectance values is negligible.

This study focused on measurements taken at the NJS located nearby the Marsdiep inlet (53°00′06″N; 4°47′21″E) to the Dutch part of the Wadden Sea (Fig. 1). The Marsdiep inlet is located at the western border and consists of a deep tidal channel flanked by shallow sand and mudflats. The inlet is bordered by the island Texel to the north and by the town of Den Helder to the south on the mainland.

3. Dataset

3.1. Time series of in-situ measurements at the NIOZ jetty station

The NIOZ jetty station (hereafter referred to as the NJS) provided the dataset of the present study. This dataset contained the time series of in-situ hyperspectral measurements of water leaving reflectance (R_{rs}) concurrent with Chla and SPM concentrations (collected at noon time almost every day) from 2008 to 2010. Fig. 2 presents the spectral variations of the in-situ R_{rs} measurements at the NJS for this study.

The NJS has been in operation since 2001 by the Royal Netherlands Institute for Sea Research (NIOZ) on the Texel Island. Every 15 min in-situ hyperspectral measurements (surface, sky and sun) including meteorological data are being collected using the newest generation of TRIOS Ramses hyperspectral radiometers (Fig. 1 bottom) for “autonomous” monitoring of seawater since August 2001 until present (Wernand, 2011). For more detailed information on the measurement setup of the NJS, the readers are referred to Wernand (2002).

3.2. Time series of tidal information at the Den Helder station

Simultaneously with recording R_{rs} measurements at the NJS, tidal measurements (water depth values, ebb and flood measurements) are recorded at Den Helder (52.9667° N, 4.7500° E) located only 3.7 km away from the NJS. Therefore, we had the opportunity to investigate the possible correlation between the tidal phase and the variation of WCCs at the NJS. In this study, three-years (2008–2010) of diurnal tidal measurements containing the water depth values in Normal Amsterdam Level (NAP) [cm] units, ebb and flood tidal phase information, besides sunrise and sunset time were extracted from the Den Helder station to make this evaluation.

4. Method

This study followed the below steps to meet the main objectives of this research:

(a) Perform data quality control of the NJS dataset.
(b) Evaluate the 2SeaColor model accuracy under different SZA conditions.
(c) Evaluate the 2SeaColor model accuracy under different water turbidity conditions.
(d) Evaluate the reliability of SIOPs measured by Hommersom et al. (2009).
(e) Analyze the effect of tide on WCC variations at the NJS.

4.1. Data quality control and R_{rs} calculations at the NJS

Ship-borne and unsupervised optical measurements collected by sensors installed on jetties, freighters or ferries can be hampered by factors like meteorological conditions, precipitation or the sun glint effect. These factors can significantly influence the radiance and irradiance measurements and consequently the accuracy of the retrieved WCCs from calculated water leaving reflectance values. Performing data quality control by data flagging (based on the knowledge under which meteorological conditions the optical measurements were collected) is crucial in water quality studies using remote sensing measurements. In this study, three different kinds of data flagging, i.e. related to “weather conditions (e.g. precipitation, wind speed)”, “spectral shape” and “sun glint contamination” were implemented to select the high-quality measurements automatically. This implemented data flagging approach was proposed by Wernand (2002), based on thousands of measurements of incident solar irradiance as well as coastal watercolor, and the meteorological dataset collected at the NJS. By implementing the precipitation flag, we indicated whether any precipitation occurred during the time of the measurements. Next, the

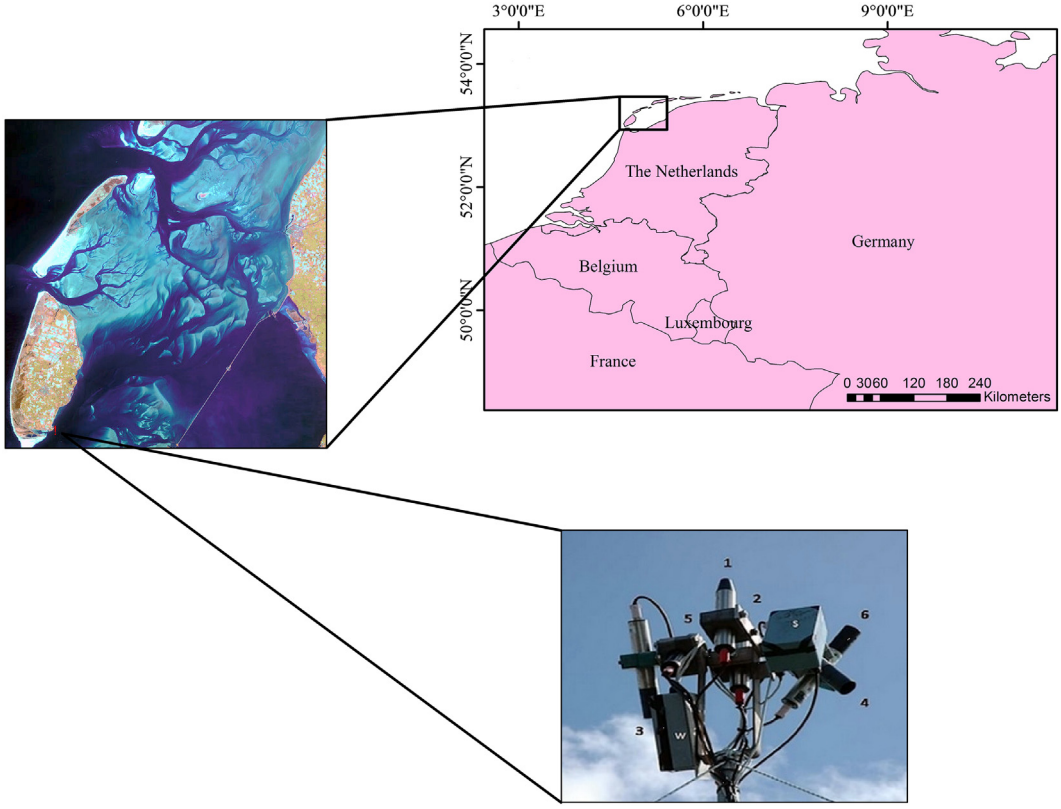

Fig. 1. Upper-right: the Southwestern part of the Dutch Wadden Sea in Europe; Upper-left: one SPOT satellite image covering the Dutch Wadden Sea and parts of IJsselmeer lake (8th of May 2006); bottom: the optical sensors installed on the NIOZ jetty station with the viewing zenith angle of 35° (w: looking at water, s: looking at sky, 1: down welling irradiance sensor at ultraviolet (E_S - UV), 2: down welling irradiance sensor (E_S), 3: the surface radiance sensor looking to South East (L_{sfc} - South East), 4: the surface radiance sensor looking to South West (L_{sfc} - South West), 5: the sky radiance sensor looking at the South East (L_{sky} - South East), 6: the sky radiance sensor looking at the South West (L_{sky} - South West)).

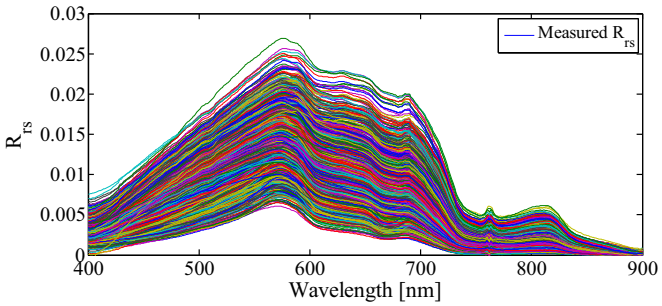

Fig. 2. The in-situ spectral measurements of R_{rs} between 2008 and 2010 at the NJS.

Table 1
Water-leaving reflectance calculation at the NJS (Wernand, 2002).

Variable	Formula	Eq.
Selecting east/west L_{sfc} sensors for R_{rs} sky correction[1]	$L_{sfc\ (min)}$ = minimum of L_{sfc} sensors	(1)
Calculate L_w	$L_w = L_{sfc\ (min)} - (f_{sky} \times L_{sky})$	(2)
Calculate R_{rs}	$R_{rs} = L_w/E_s$	(3)

[1] When L_{sfc} west was minimum, L_{sky} west was used to do sun glint contamination correction and vice-versa.

spectral shape flag detected those spectra, which were possibly influenced by specific dusk or dawn radiation (red coloring of the sky) using the band ratio of down-welling solar irradiance (E_S) values. By implementing these two data flaggings, all unacceptable spectra were removed from the dataset. However, sun glint contamination might still influence the quality of measured R_{rs} data (Wang and Bailey, 2001). To minimize the sun glint effect, the NJS was equipped with three optical hyperspectral sensors consisting of two down-looking water leaving radiance sensors (L_{sfc}), 90° apart in the horizontal plane (under azimuth angles of 135° and 225° from north), instead of the conventional single sensor measurement, as well as one down-welling irradiance (E_S) sensor (Fig. 1 bottom). In this way, one of the two water-leaving radiance signals was always available with a minimum of sun glint (Table 1), and the effect of sun glint contamination was removed from the dataset (Wernand, 2002). After performing the mentioned data quality control process and extracting the high-quality spectra from all three sensors, the water leaving reflectance values were calculated following Wernand (2002), as explained in Table 1:

The calculated in-situ R_{rs} values using the equations mentioned above in Table 1 were later used to perform WCC retrievals using the 2SeaColor model as described below.

4.2. The 2SeaColor model forward modeling and inversion scheme

Table 2 presents the employed algorithms for the 2SeaColor parameterization in this study. The same set-up of Table 2 was successfully used in previous studies for the 2SeaColor model to retrieve WCCs from remote sensing observations at the NJS (Arabi et al., 2016). Some of the employed parameterizations are of an empirical nature and therefore only valid for given ranges of the independent variables (WCCs). For instance, the Lee et al. (1999) model (Eq. (5)), is not valid for very low values of Chla (< 0.4 [mg m^{-3}]). Therefore, special care was taken to ensure that each variable stayed within its valid range, and outside these ranges, the border value was taken. To do this, we implemented

Table 2
Summary of the used parameterizations (Arabi et al., 2016).

Variable	Parameterization	Ref.	Eq.
Chla absorption[a] at λ_1	$a_{Chla}(\lambda_1) = 0.06 \times ([Chla])^{0.65}$	(Lee et al., 1999)	(4)
Chla absorption[b]	$a_{Chla}(\lambda) = \{[a_0(\lambda) + a_1(\lambda) \times \ln a_{Chla}(\lambda_1)] \times a_{Chla}(\lambda_1)\}$	(Lee et al., 1999)	(5)
CDOM absorption[c]	$a_{CDOM}(\lambda) = a_{CDOM}(\lambda_2) \times \exp[-S_{CDOM}(\lambda - \lambda_2)]$	(Bricaud et al., 1981)	(6)
NAP absorption[d] at λ_2	$a_{NAP}(\lambda_2) = a^*_{NAP}(\lambda_2) \times [SPM]$	(Lee et al., 1998)	(7)
NAP absorption[e]	$a_{NAP}(\lambda) = a_{NAP}(\lambda_2) \times \exp[-S_{NAP} \times (\lambda - \lambda_2)]$	(Lee et al., 1998)	(8)
Chla backscattering at λ_3	$b_{b,\ Chla}(\lambda_3) = 0.416 \times [Chla]^{0.766}$	(Morel and Maritorena, 2001)	(9)
Chla backscattering	$b_{b,\ Chla}(\lambda) = \{0.002 + 0.01 \times [0.5 - 0.25 \times \log_{10}[Chla] \times (\lambda/\lambda_3)^n]\} \times b_{b,\ Chla}(\lambda_3)$	(Morel and Maritorena, 2001)	(10)
NAP backscattering[f] at λ_3	$b_{NAP}(\lambda_3) = b^*_{NAP}(\lambda_3) \times I \times [SPM]$	(Doxaran et al., 2009a, 2009b)	(11)
NAP scattering[g]	$b_{NAP}(\lambda) = b_{NAP}(\lambda_3) \times (\lambda_3/\lambda)^{\gamma} - [1 - \tanh(0.5 \times \gamma^2)] \times a_{NAP}(\lambda)$	(Doxaran et al., 2009a, 2009b)	(12)
Water molecules absorption[h]	$a_W(\lambda)$: listed values	(Pope and Fry, 1997)	(13)
Water molecules scattering	$b_{bw}(\lambda)$: listed values, table (3.8), page 104.	(Mobley, 1994)	(14)
Total absorption coefficient	$a(\lambda) = a_W(\lambda) + a_{Chla}(\lambda) + a_{NAP}(\lambda) + a_{CDOM}(\lambda)$	(IOCCG, 2000)	(15)
Total backscattering coefficient	$b_b(\lambda) = b_{bw}(\lambda) + b_{b,\ Chla}(\lambda) + b_{b,\ NAP}(\lambda)$	(Arnone et al., 2006)	(16)
Backscattering to absorption coefficients ratio	$x = b_b/a$	(Salama and Verhoef, 2015)	(17)
The directional-hemispherical reflectance of the semi-infinite medium[i]	$r^{\infty}_{sd} = (\sqrt{1 + 2x} - 1)/(\sqrt{1 + 2x} + 2\mu_w)$	(Salama and Verhoef, 2015)	(18)
Irradiance reflectance beneath the surface[j]	$R(0^-) \simeq r_{sd}{}^{\infty}/Q$	(Mobley et al., 1993)	(19)
Above-surface remote sensing reflectance	$R_{rs} = (0.52 \times R(0^-))/(1 - 1.7 \times R(0^-))$	(Lee et al., 2002)	(20)

[a] λ_1, λ_2 and λ_3 are reference wavelengths at 443, 440 and 550 nm, respectively.
[b] a_0 and a_1 are the absorption and backscattering coefficients of water molecules taken from Lee et al. (1998).
[c] $S_{CDOM} = 0.013$ [nm^{-1}] is the spectral slope of *CDOM* taken from Hommersom et al. (2009).
[d] $a_{NAP}{}^*(\lambda_2) = 0.036$ [$m^2\ g^{-1}$] is the specific absorption of non-algae particles taken from Hommersom et al. (2009).
[e] $S_{NAP} = 0.011$ [nm^{-1}] is the spectral slope of non-algae particles (*NAP*) taken from Hommersom et al. (2009).
[f] $b_{NAP}{}^*(\lambda_3) = 0.282$ [$m^2\ g^{-1}$] is the specific scattering coefficient of *NAP* taken from Hommersom et al. (2009) and $I = 0.019$ for the North Sea was taken from Petzold (1972).
[g] $\gamma = 0.6$ for the North Sea was taken from Doxaran et al. (2009a, 2009b).
[h] a_w and b_{bw} are the absorption and backscattering coefficients of water molecules and were taken from Mobley (1994) and Pope and Fry (1997).
[i] μ_w is the cosine of the SZA below the (flat) water surface.
[j] $Q = 3.25$ was taken from Mobley (1994).

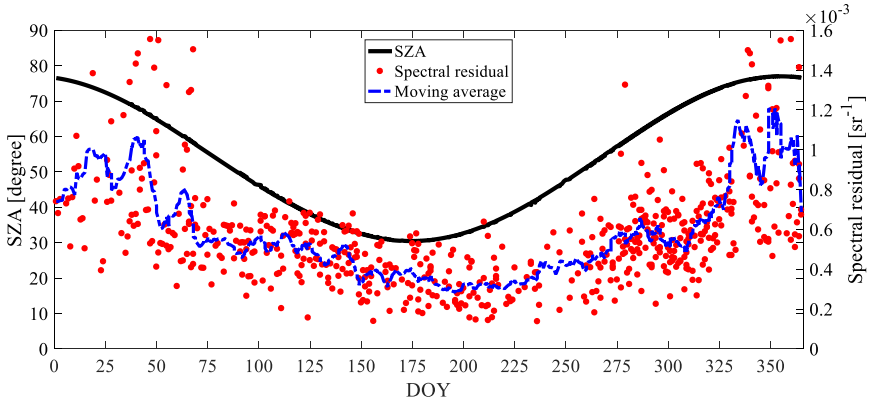

Fig. 3. The spectral residual (RMSE between the best fits of modeled and measured R_{rs}) and the yearly SZA variation versus DOY for the quality-controlled meteorological, shape and sun glint effect dataset between 2008 and 2010 at the NJS.

an automatic truncation function in MATLAB to stay within the valid ranges of WCCs in this study.

In Table 2, the symbols a and b_b represent the absorption and backscattering coefficients. The subscripts *Chla*, *SPM*, *CDOM*, *NAP* and *W* denote Chlorophyll-a, Suspended Particulate Matter, Colored Dissolved Organic Matter, Non-Algae Particles (NAP) and water molecules, respectively. [*Chla*], [*SPM*] are the concentrations corresponding to Chla and SPM, respectively. It should be noted that the predicted reflectance from the water by the 2SeaColor model ($r_{sd}{}^{\infty}$) is dependent on the SZA values (Eq. (18)), although the range in the cosine of the SZA (μ_w) is quite moderate, since the maximum SZA under water is Brewster's angle, 53° for water. The calculated IOPs using the parameterizations in Table 2 and the set of measured SIOPs valid for the Dutch Wadden Sea were used to model R_{rs} spectra by the 2SeaColor model (Eqs. (17)–(20)). Next, an iterative optimization technique was applied for the model inversion to retrieve the WCCs. Within the constraints mentioned in Table 2, there are three WCCs in Eq. (18), Chla [$mg\ m^{-3}$] concentration, SPM [$g\ m^{-3}$] concentration and CDOM absorption at 440 nm [m^{-1}], which uniquely determine the modeled R_{rs} spectra. These unknown variables can be retrieved by minimizing the differences between R_{rs} curves that are modeled by the 2SeaColor model calculated in Eq. (20) and the measured ones calculated in Eq. (3) (Lee et al., 1999). The "Trust Region" algorithm, implemented in the MATLAB (The MathWorks, Inc. Natick, MA, USA) function

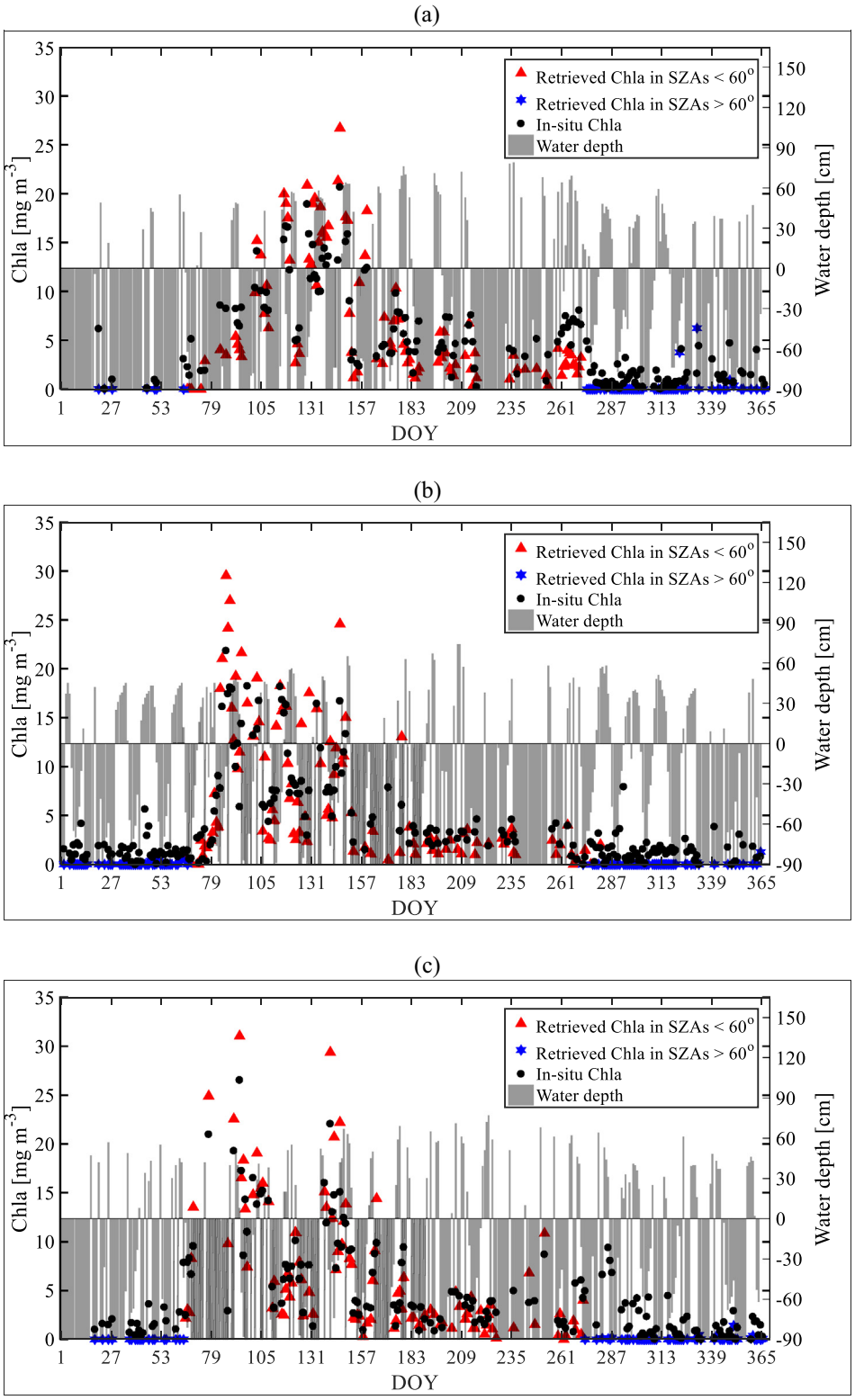

Fig. 4. Temporal variation of retrieved Chla concentrations [mg m^{-3}] by the 2SeaColor model versus in-situ Chla concentrations [mg m^{-3}] for the flagged meteorological, shape and sun glint effect dataset at the NJS in (a): 2008; (b): 2009 and (c): 2010.

"lsqnonlin", was used to minimize the cost function. The program calculated the Root Mean Square Error (RMSE) between the measured and modeled values over the whole wavelength range of the reflectance spectra.

To avoid local minima, we did the minimization in numerous loops starting with different WCCs initial guesses as recommended by Salama and Shen (2010). We changed the model's initial values and modeled the R_{rs} spectra. The results (data are not shown) showed that initial values had no significant effects on the minimization and thus on the retrieved parameters.

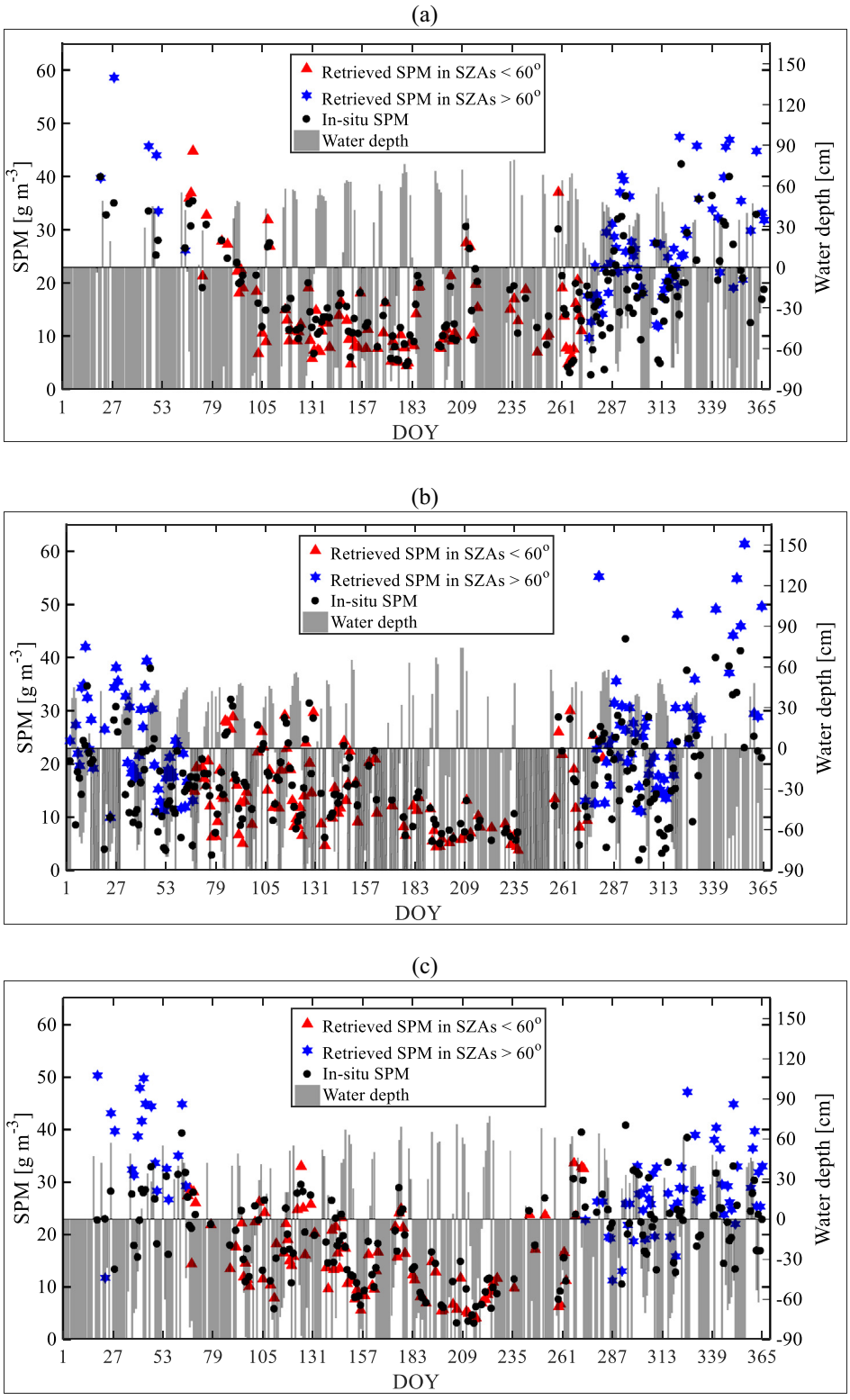

Fig. 5. Temporal variation of retrieved SPM concentrations [g m^{-3}] by the 2SeaColor model versus in-situ SPM concentrations [g m^{-3}] for the flagged meteorological, shape and sun glint effect dataset at the NJS (a): 2008; (b): 2009 and (c): 2010.

4.3. Evaluation of the 2SeaColor model accuracy under different SZA values, turbidity conditions and set of measured SIOPs at the NJS

To investigate the SZA variation effect, we categorized the time series of in-situ R_{rs} measurements into different SZA groups. Considering the yearly SZA variation (from 30° to 75°) at the measurement site (located at 53° North) with an average change of almost 7.5° per month, we created six SZA groups (SZAs < 37.5°, 37.5° ≤ SZAs < 45°, 45° ≤ SZAs < 52.5°, 52.5° ≤ SZAs < 60°, 60° ≤ SZAs < 67.5° and 67.5° ≤ SZAs ≤ 75°). Regarding different water turbidity conditions, we extracted the concentration ranges of in-situ Chla [mg m^{-3}] and SPM [g m^{-3}] measurements between 2008 and

Table 3
The initial guess of WCCs used in the model inversion.

Variable	Unit	Lower/upper boundary	Border values	Initial guess
Chla	$mg\,m^{-3}$	0–50	0, 50	0.1
SPM	$g\,m^{-3}$	0–100	0, 100	20
CDOM	m^{-1}	0–3	0, 3	0.25

Table 4
The statistical measures used for evaluation of the SZAs effect on the retrieved Chla [$mg\,m^{-3}$] concentrations by the 2SeaColor model.

SZAs	R^2	Unequal standard deviations (%)	Bias in the mean values (%)	Lack of (positive) correlation (%)	Total MSE
[30°–37.5°)	0.81	18.15	0.15	81.69	6.61
[37.5°–45°)	0.78	18.17	2.15	79.68	7.43
[45°–52.5°)	0.74	28.67	4.72	66.61	11.44
[52.5°–60°)	0.72	14.77	20.00	65.23	8.80
[60°–67.5°)	0.03	50.12	43.93	15.95	8.40
[67.5°–75°]	0.08	42.30	43.40	14.30	10.07

Table 5
The statistical measures used for evaluation of the SZAs effect on the retrieved SPM [$g\,m^{-3}$] concentrations by the 2SeaColor model.

SZAs	R^2	Unequal standard deviations (%)	Bias in the mean values (%)	Lack of positive correlation (%)	Total MSE
[30°–37.5°)	0.89	1.69	21.01	77.29	4.14
[37.5°–45°)	0.84	1.54	10.57	87.89	8.42
[45°–52.5°)	0.83	1.46	10.41	88.13	10.28
[52.5°–60°)	0.87	1.52	14.35	84.14	11.85
[60°–67.5°)	0.23	0.58	31.97	67.45	36.25
[67.5°–75°]	0.42	0.74	41.20	58.06	65.09

2010 at the NJS corresponding to each SZA group separately. Then a Mean Squared Error (MSE) decomposition analysis was performed for different SZA groups and water turbidity conditions at the NJS. The MSE is one of the most widely used criteria for evaluation of models against in-situ measurements. We decomposed the MSE into three contributions due to i) unequal standard deviations, ii) a bias in the mean values, and iii) a lack of (positive) correlation, following (Gupta et al., 2009) as expressed in Eq. (21).

$$MSE = (\sigma_1 - \sigma_2)^2 + (\mu_1 - \mu_2)^2 + 2\sigma_1\sigma_2(1 - R) \quad (21)$$

where 1 and 2 indicate the variables (modeled and measured values), σ and μ are standard deviations and means, respectively, and R is the correlation coefficient. The results of the MSE decomposition analysis results are presented in Sections 5.1 and 5.2. Finally, we analyzed the reliability of measured SIOPs to be implemented in the 2SeaColor model parametrization at the NJS. For this evaluation, the occurrence of any systematic errors between modeled and measured R_{rs} spectra in different parts of the spectrum by using the spectral difference criteria for different SZA groups was investigated. Results of this evaluation are also presented in Section 5.3.

4.4. The 2SeaColor model validation

The 2SeaColor model accuracy was evaluated at two different levels: (i) validating the modeled spectra against in-situ R_{rs} measurements at the four reference wavelengths of 443, 490, 550 and 665 nm and (ii) validating the retrieved concentrations of Chla and SPM against in-situ measurements. The statistical measures of the determination coefficient (R^2) and the Root Mean Square Error (RMSE) were used to quantify the goodness-of-fit between modeled and measured R_{rs}, and retrieved and measured in-situ Chla and SPM concentrations. The results of these assessments are presented in Section 5.4.

4.5. Tidal effect evaluation

For the tidal effect evaluation, two different approaches were used in this study. In the first approach, the temporal variation of in-situ SPM and Chla concentrations corresponding to their water depth values within the yearly tidal cycles between 2008 and 2010 at the NJS were plotted (Figs. 4 and 5). Next, the correlation between time series of in-situ Chla and SPM concentrations at the NJS and the corresponding water depth values at the Den Helder station for different SZA groups was calculated to investigate the possible correlation between these two parameters (Table 10). For the second approach, a complete dataset of ebb and flood tidal information (including water depth values during the ebb and flood, ebb and flood occurrence times and sunrise and sunset time per day) between 2008 and 2010 were obtained for the Den Helder station (flood: 1076 measurements, ebb: 1065 measurements). For times concurrent with tidal events, in-situ R_{rs} measurements at the NJS were extracted. After performing the data quality control process, 508 and 383 reliable in-situ R_{rs} measurements were selected under conditions of flood and ebb, respectively. Then, the 2SeaColor model was inverted to retrieve Chla and SPM concentrations per each R_{rs} measurement of the quality-controlled dataset. Then the differences between mean values of retrieved SPM and Chla concentration during flood and ebb for different SZA groups were evaluated as an indicator to investigate whether the tide causes any significant change in the WCCs (Table 11).

5. Results

5.1. Evaluation of the 2SeaColor model accuracy under different SZA conditions

Fig. 3 presents the daily variation of SZA over the year at the NJS. The spectral residuals (RMSE) between in-situ and modeled R_{rs} values over the whole wavelength region as a function of time (DOY) are also presented in this figure.

The X-axis in this figure shows DOYs during three years (between 2008 and 2010). The left Y-axis shows the SZA values corresponding to each day (black line). The spectral residual (RMSE) values for each measurement are presented with red dots while a moving average with a span of 5 days is also used (blue dashed-line) to show the variation of RMSE with SZA variation better. As the figure shows, the spectral residual values increase (from 0.0001 to 0.0016 [sr^{-1}]) nearly in parallel with SZA (from 10° to 80°). By evaluating the rising trend of spectral residual amounts at high SZAs (SZAs > 60°), it can be concluded that the 2SeaColor model inversion yields worse spectral fitting results under high SZAs in this region. As to the effect of SZA variation on the accuracy of the 2SeaColor model retrievals, the results of MSE decomposition analysis for all SZA groups are computed in Tables 4 and 5. In these tables, the distribution of the three error sources (i.e. unequal standard deviations (second column), bias in the mean values and lack of correlation (third column) and lack of correlation (fourth column)) are calculated as the percentages (%) of total MSE. In addition, the calculated R^2 values (first column) are attached to the MSE decomposition tables as follows:

As the results of Table 4 show, the calculated R^2 values between the measured and retrieved Chla estimates significantly decrease (from 0.81 to 0.08) when SZAs become higher than 60°. The R^2 value of Chla is around 0.80 for 30° < SZAs < 52°, decreasing to 0.75 for 52° < SZAs < 60° and it is dropping to < 0.2 for SZAs > 60°. Therefore, the SZA of 60° might be considered as a threshold which leads to less accurate retrievals in case R_{rs} measurements are collected at SZAs > 60°. However, the total MSE values for all SZA groups are relatively small (between 6 and 12) and do not increase in parallel with the SZA. The very low R^2 values (< 0.1) of Chla retrievals by the model

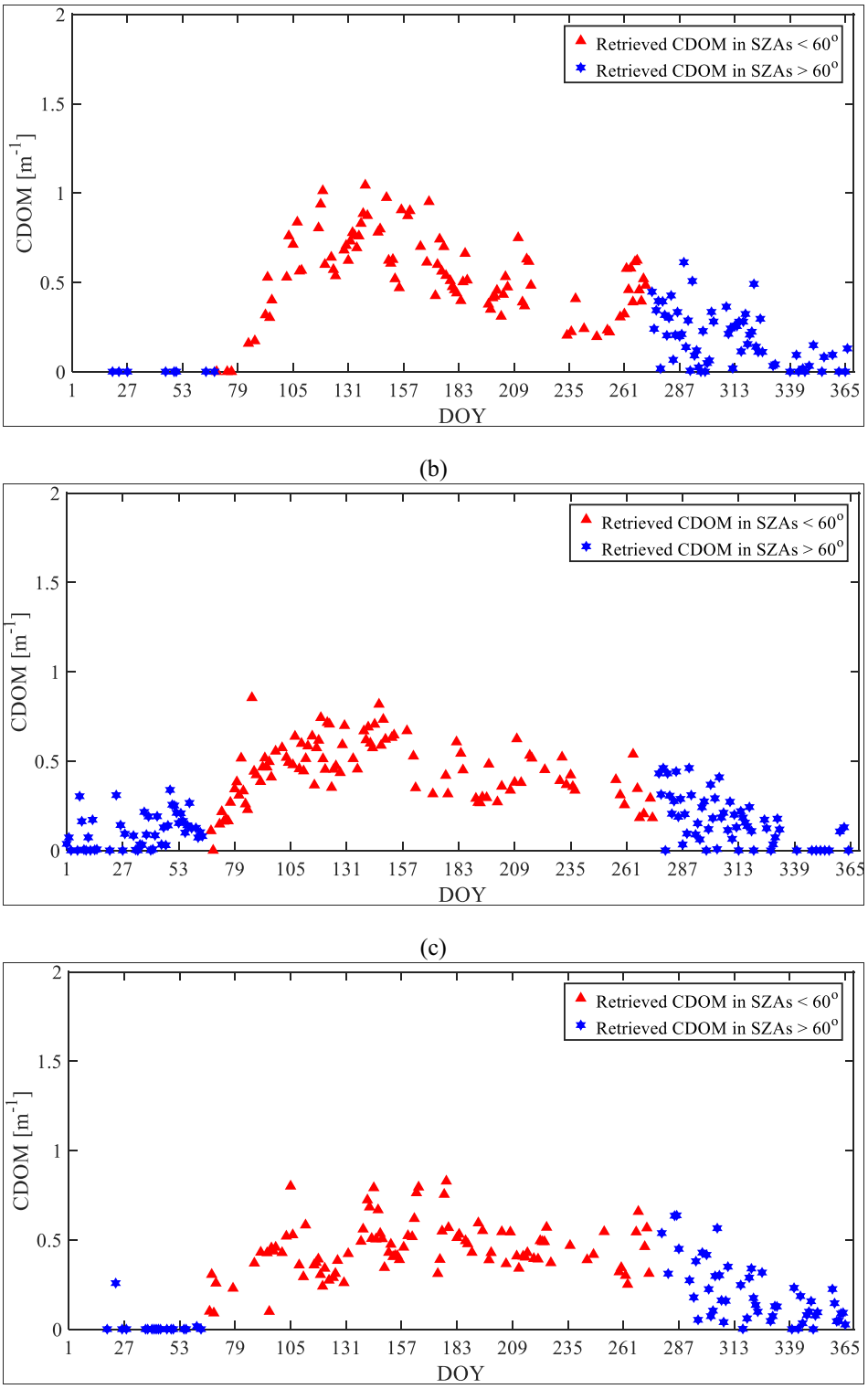

Fig. 6. Temporal variation of retrieved CDOM absorption at 440 nm [m^{-1}] by the 2SeaColor model for the flagged meteorological, shape and sun glint effect dataset at the NJS (a): 2008; (b): 2009 and (c): 2010. (For interpretation of the references to color in this figure, the reader is referred to the web version of this article.)

in winter (SZAs > 60°) do contribute little (< 15%) to the total MSE and therefore cannot be considered a major source of error. This also means that R^2 as an error measure is rather meaningless in this case. Improving the correlation would not help much here since the greatest contributions to the MSE decomposition for Chla estimates in winter (SZAs > 60°) come from the bias in the mean values (~45%) and the unequal standard deviations (~50%) while the lack of positive correlation plays the smallest role (~15%) in the total MSE. The results of the calculated R^2 values as well as the MSE decomposition analysis for all SZA groups for SPM estimates are presented in Table 5.

Like for the Chla estimates, the calculated R^2 values between the measured and retrieved SPM estimates significantly decrease (from 0.89 to 0.42) in winter when SZAs become higher than 60°. On the other hand, the total MSE values of SPM estimates also increase (from 4

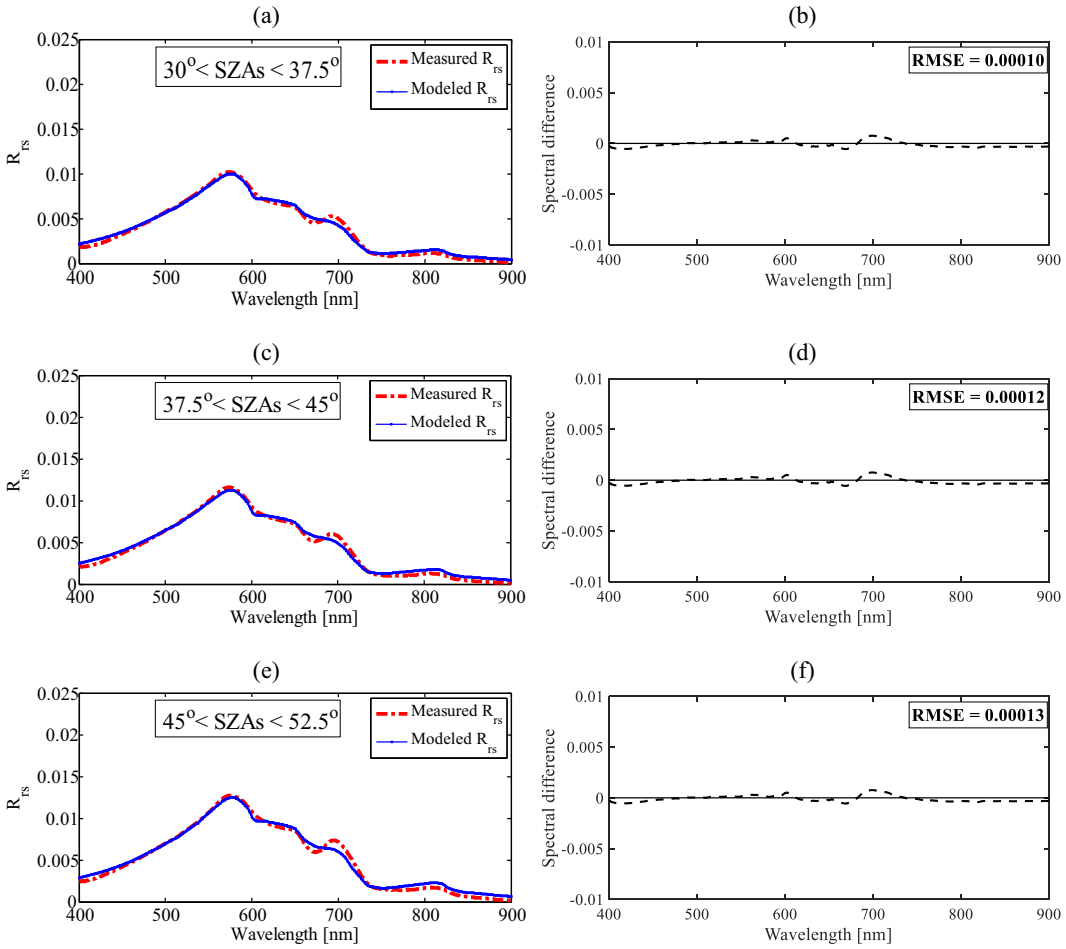

Fig. 7. The spectral differences between in-situ and model's best fit R_{rs} corresponding to the different SZA groups versus wavelength for the quality-controlled meteorological, shape and sun glint effect dataset between 2008 and 2010 at the NJS. Left: red dashed-lines present the spectral average of in-situ R_{rs} values and the blue lines present the spectral average of the models best fits R_{rs} values; right: the spectral differences (RMSE) between in-situ and model's best fit R_{rs} for the whole wavelength region. (a,b): data collected at SZAs [30°–37.5°); (c,d): data collected at SZAs [37.5°–45°); (e,f): data collected at SZAs [45°–52.5°); (g,h):data collected at SZAs [52.5°–60°); (i,j): data collected at SZAs [60°–67.5°); (m,n): data collected at SZAs [67.5°–75°]. (For interpretation of the references to color in this figure legend, the reader is referred to the web version of this article.)

to 65) with the SZA increase in winter. The total MSE values are ~12 for SZAs $<$ 60° and they increase dramatically to ~65 for SZAs $>$ 60°. Moreover, the lack of positive correlation does have the most significant contribution (~70%) to the total MSE for SPM estimates in winter. Therefore, the seasonal variation of higher SPM concentrations in winter might be another factor besides the SZA effect that leads to the sudden increase of total MSE at SZAs $>$ 60°. In the following section, the 2SeaColor model's performance with respect to the variation range of in-situ Chla and SPM concentrations at different SZA groups is investigated.

5.2. Evaluation of the 2SeaColor model performance under different water turbidity conditions

The ranges of in-situ Chla and SPM concentrations for the various SZA groups at the NJS are presented in Table 6:

As can be seen from Table 6, the maximum levels of in-situ SPM concentrations (~50 [g m^{-3}]) occur during winter (SZAs $>$ 60°) while these amounts are considerably higher than the maximum levels of SPM concentration (~ 30 [g m^{-3}]) during spring and summer (30° $\leq$ SZAs $<$ 52.5°). Conversely, the maximum levels of in-situ Chla concentration (~30 mg m^{-3}) occur in spring and summer, while these amounts reach their minimum values (~0.1 [mg m^{-3}]) during winter. Therefore, the substantial variations in concentration of in-situ measured Chla and SPM in different seasons in the NJS might be another reason for the model's deterioration in winter, especially for the SPM estimates. Figs. 4 and 5 present the temporal variation of retrieved Chla and SPM concentration versus their corresponding in-situ measurements at the NJS. In these figures, the retrieved values between March and October (SZAs $<$ 60°) are shown by red triangles. Blue stars show the retrieved values during winter (SZAs $>$ 60°), and black dots indicate the in-situ Chla and SPM measurements at the NJS. In addition, the water depth values at the Den Helder station corresponding to each in-situ Chla and SPM measurement at the NJS are presented in grey bars to support the further analysis given in Section 5.5.

As can be seen in Fig. 4, the temporal trends of retrieved and in-situ Chla concentrations [mg m^{-3}] are in good agreement (between 0 and 35 [mg m^{-3}]) with the daily Chla concentration variations between 2008 and 2010 at the NJS. The highest values of retrieved and measured Chla concentrations are mainly observed in the spring period (April, May, and June) ~30 [mg m^{-3}]. After the spring period, Chla values start to decrease in July (~5 [mg $^{-3}$]) with a slight increase in September (~10 [mg m^{-3}]), and they reach their lowest values during winter (~0 [mg m^{-3}]) (blue stars). However, underestimation of retrieved Chla concentrations in comparison to in-situ measurements in winter (SZAs $>$ 60°) can be observed in all three years (Fig 4(a), (b) and (c)). Indeed, the low concentration of in-situ Chla measurements during the winter makes the water leaving spectrum less sensitive to

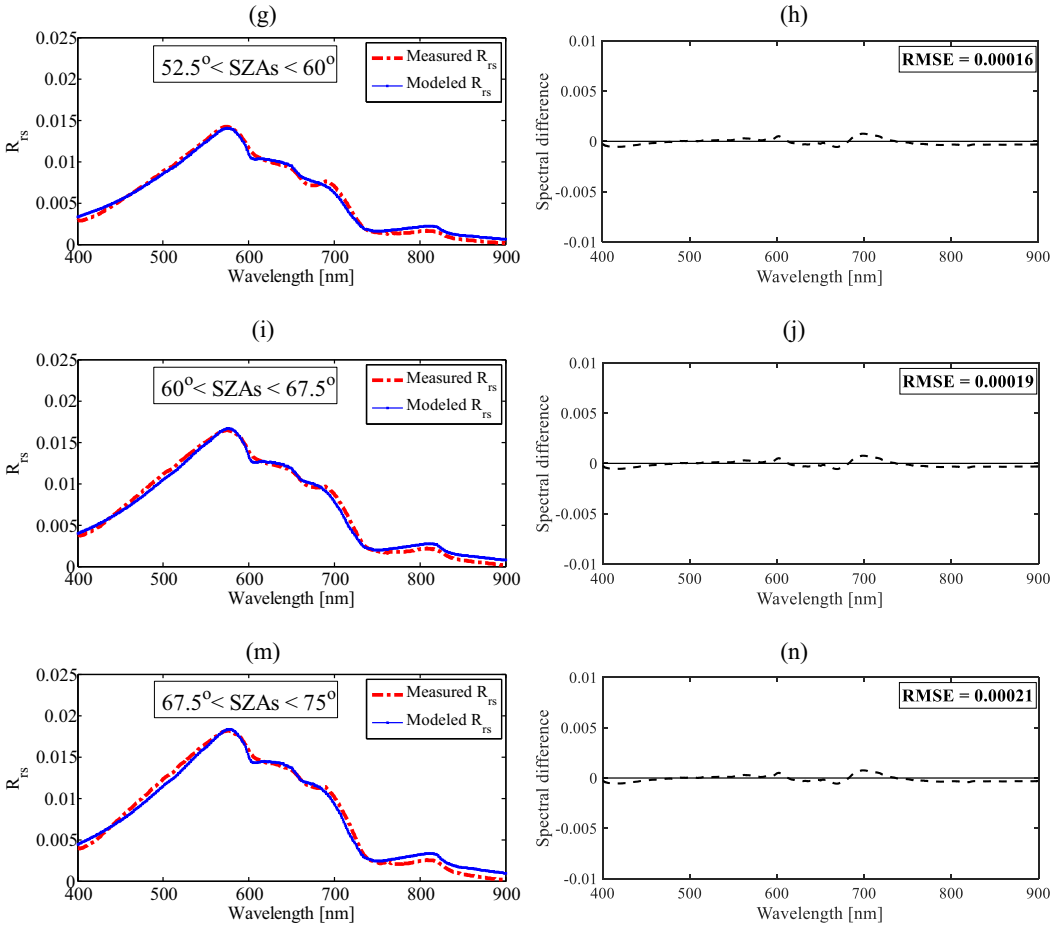

Fig. 7. (*continued*)

Table 6
The concentration ranges of in-situ Chla [mg m^{-3}] and SPM [g m^{-3}] measurements corresponding to each SZA group between 2008 and 2010 at the NJS.

SZAs	Chla	SPM
[30°–37.5°)	0.22–22.04	3.06–30.54
[37.5°–45°)	1.37–18.92	5.60–31.39
[45°–52.5°)	0.84–26.52	7.64–32.08
[52.5°–60°)	0.19–20.96	2.84–39.46
[60°–67.5°)	0.19–09.37	3.63–43.48
[67.5°–75°]	0.40–08.51	1.17–51.65

changes in Chla values. That is why the model underestimates Chla concentration retrievals by tending to take the lower boundaries (~0 [mg m^{-3}]) of the Chla concentration variable through optimization techniques (Table 3). On the other hand, in-situ Chla concentrations occur in very low ranges (~0 to 5 [mg m^{-3}]) during winters. Consequently, reasonable temporal agreement occurs between the retrieved and in-situ Chla concentrations in winter, with relatively low total MSE (~10) in the high SZA groups (SZAs > 60°) (Table 4), which also means that the low R^2 (< 0.1) is harmless in wintertime, since the low Chla concentrations in winter (between 0 and 5 [mg m^{-3}]) were predicted correctly. Therefore, it can be concluded that the 2SeaColor model is capable enough to retrieve Chla concentrations under different water turbidity conditions at the NJS. The temporal variations of retrieved SPM concentrations versus in-situ ones at the NJS are presented in Fig. 5.

As can be seen in Fig. 5, the temporal trends of retrieved and in-situ SPM concentrations [g m^{-3}] are in good agreement (between 0 and 60 [g m^{-3}]) with the daily water turbidity variation between 2008 and 2010 at the NJS. Both retrieved and in-situ SPM concentrations show their highest values (between 10 and 60 [g m^{-3}]) from January to February, they start to decrease (from 0 to 30 [g m^{-3}]) from April to July and they increase again at the beginning of October (between 10 and 35 [g m^{-3}]), until they reach their highest level in November and December (between 40 and 60 [g m^{-3}]). On the other hand, some overestimation of retrieved SPM concentrations in comparison to in-situ measurements can be observed during winters (SZAs > 60°) in all three years. As the results of the MSE analysis also showed (Table 5), the total MSEs significantly (from 4 to 65 [g m^{-3}]) increase in winter, in parallel with SZA increase (from 30° to 75°) while the most significant contribution to this error at SZAs > 60° is due to lack of correlation (~90%). Therefore, the higher level of SPM concentrations in winter in comparison to summer level (SZAs < 60°) might be another reason (besides SZA increase) that the total MSE values considerably increase during winter for SPM retrievals (from 4 to 65 [g m^{-3}]). However, as explained before in Section 1.2, and following recent studies (Arabi et al., 2016; Salama and Verhoef, 2015; Yu et al., 2016a), the 2SeaColor model has been developed to deal with high turbidity. Therefore, this SPM overestimation might be related to the unreliability of the SIOPs implemented in the 2SeaColor model's parametrization for SPM retrievals during winter. The main reason is that the SPM concentration levels follow a certain seasonal pattern over different years (Fig. 5(a), (b), (c)) while there is no information about seasonal SIOPs at this moment for the NJS. Indeed, the implemented SIOPs in this study have been collected only during spring and summer (Hommersom et al., 2010). However, even this model overestimation in winter still shows fairly reasonable agreement with the trend of in-situ SPM concentrations for all three years. Therefore, from the results of this

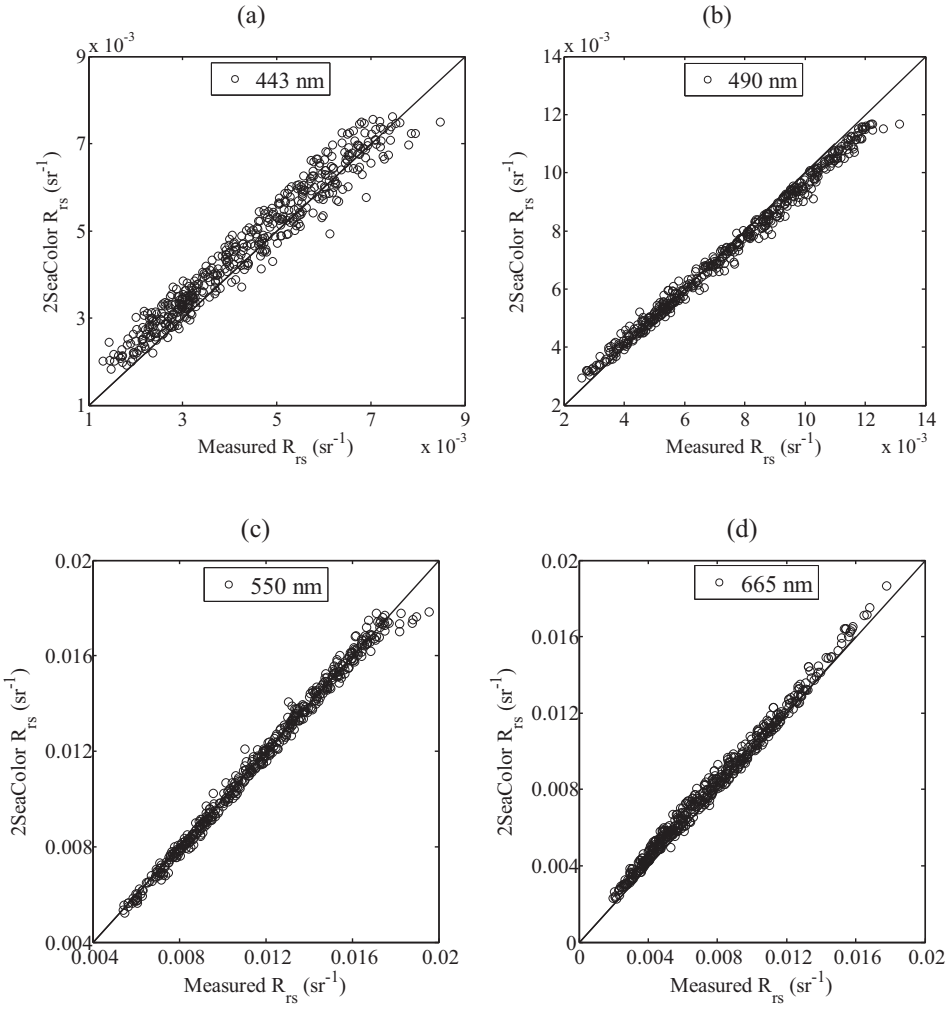

Fig. 8. Comparison between the 2SeaColor model's best-fit spectra and in-situ R_{rs} measurements for the quality-controlled dataset between 2008 and 2010 at the NJS for wavelengths: (a) 443 nm; (b) 490 nm; (c) 550 nm and (d) 665 nm.

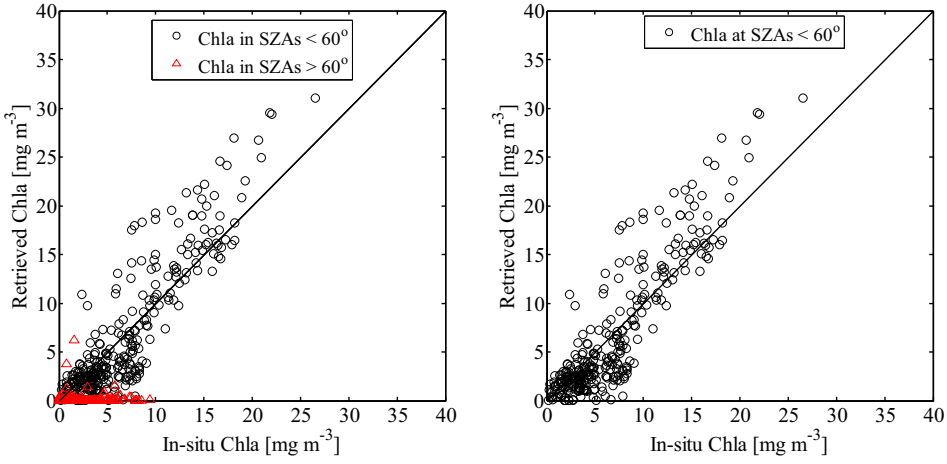

Fig. 9. Left: comparison between retrieved and in-situ measurements of Chla concentration [mg m^{-3}] for the quality-controlled dataset between 2008 and 2010 at the NJS; right: the same after removing winter retrievals.

evaluation it can be concluded that the 2SeaColor model is capable enough to retrieve SPM concentrations under various water turbidity conditions at the NJS. However, the results of winter retrievals (SZAs > 60°) show a considerable model overestimation in this season. It should be noted that the 2SeaColor model also retrieves CDOM absorption at 440 nm [m^{-1}] simultaneously with Chla and SPM concentration values. The trend of retrieved CDOM by the 2SeaColor model is presented in Fig. 6. However, there were no in-situ CDOM measurements to evaluate the agreement between the temporal variation of measured and retrieved CDOM absorptions.

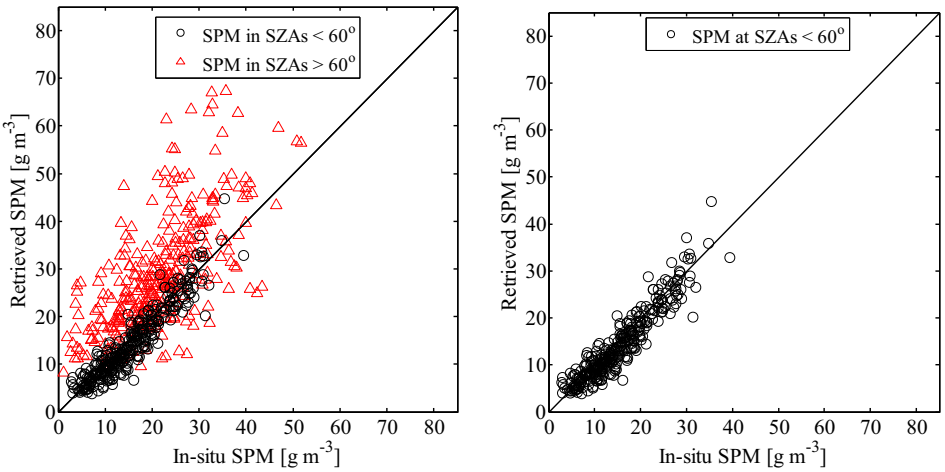

Fig. 10. Left: comparison between retrieved and in-situ measurements of SPM concentration [g m^{-3}] for the quality-controlled dataset between 2008 and 2010 at the NJS; right: the same after removing winter retrievals.

Table 7
The model's performance evaluation for R_{rs} model's best-fit spectra against in-situ ones for the quality-controlled dataset between 2008 and 2010 at the NJS for wavelengths at 443, 490, 550 and 665 nm.

Wavelength/statistical measures	R^2	RMSE [sr^{-1}]
443 nm	0.95	0.00032
490 nm	0.99	0.00019
550 nm	0.99	0.00028
665 nm	0.99	0.00032

Table 8
The model's performance evaluation of Chla retrievals for the quality-controlled dataset with and without winter retrievals between 2008 and 2010 at the NJS.

SZA groups/statistical measures	R^2	RMSE [mg m^{-3}]
All dataset (Fig. 9 left)	0.79	2.57
SZAs < 60° (Fig. 9 right)	0.80	2.98

Table 9
The model's performance evaluation of SPM retrievals for the quality-controlled dataset between 2008 and 2010 at the NJS.

SZA groups/statistical measures	R^2	RMSE [g m^{-3}]
All dataset (Fig. 10 left)	0.66	7.65
SZAs < 60° (Fig. 10 right)	0.89	2.53

As Fig. 6 shows, the temporal variability of CDOM is independent of that of Chla (Yu et al., 2016b). In general, the retrieved values of CDOM (blue stars) are low (~0.5 m^{-1}) during winter (SZAs > 60°) and increasing to ~1.2 m^{-1} in spring and summer (red triangles) during three years at the NJS. Moreover, the temporal CDOM absorption variations follow similar trends [between 0 and 2 m^{-1}] over the years between 2008 and 2010 at the NJS.

5.3. Evaluation of the reliability of the set of measured SIOPs at the NJS

The reliability of the measured SIOPs by Hommersom et al. (2009) used in the 2SeaColor model parametrization, are evaluated as explained in Fig. 7.

As the left panels of this figure show, by using Hommersom's SIOPs, good fits are found between measured and modeled R_{rs} spectra while the calculated RMSE are in very low range groups (0.0001 < RMSE < 0.00022) for all SZA. However, as the right panels of this figure show, many zero-crossings occur constantly at nearly the same spectral positions. For example, there are systematic R_{rs} underestimations around 410 and 600 nm for all SZA groups. In addition, another systematic R_{rs} overestimation can be observed in the Near Infrared Red (NIR) part of the spectrum (between 780 and 900 nm). Regarding the similar patterns of zero-crossings as well as the very low spectral residuals (0.0001 < RMSE < 0.00022) for all SZA groups (Fig. 7 right panel), it can be stated that the SIOPs measured by Hommersom et al. (2009) are suitable to be implemented for the 2SeaColor model parametrization at the NJS. However, there is a slight mismatch between the real and implemented SIOPs for the 2SeaColor model parametrization at this region. Therefore, modifying these SIOPs with respect to the seasonal patterns of WCCs at the NJS may lead to improved retrieval results. On the other hand, as the right panels of Fig. 7 show, the calculated RMSE values between the measured and modeled R_{rs} spectra increase (from 0.00010 to 0.00021) in parallel with the SZA increase (from 30° to 75°). The RMSE values are around 0.00013 for 30° < SZAs < 52°, increasing to 0.00016 for 52° < SZAs < 60° and rising to around 0.0002 for SZAs > 60°. On the other hand, the amplitudes of R_{rs} values also increase (from 0.01 to 0.02) (Fig. 7, left panels) in parallel with the SPM level increase from spring to winter (Table 6). The R_{rs} amplitude values are around 0.012 for 30° < SZAs < 52°, increasing to 0.015 for 52° < SZAs < 60° and are rising to around 0.02 for SZAs > 60°. This can be other evidence of the lower reliability of the retrieved WCCs during winter under high SZA conditions at the NJS (Table 5). However, it is uncertain whether the higher spectral residuals and consequently the worse retrieval results during winter are caused by the seasonal pattern of SPM concentrations and lack of seasonal SIOPs, or by the SZA effect.

5.4. Validation of the 2SeaColor model performance to model R_{rs} spectra and retrieve WCCs against in-situ measurements

The results of the 2SeaColor model validation for modeling R_{rs} spectra and retrieving Chla and SPM concentrations are provided in Figs. 8, 9 and 10, respectively.

Fig. 8 presents the results of the 2SeaColor model validation for modeling R_{rs} spectra for the four wavelengths at 443, 490, 550 and 665 nm for the flagged meteorological, shape and sun glint effect dataset between 2008 and 2010 at the NJS. As this figure shows, the modeled best fitting spectra agree very well with measured spectra at the selected wavelengths. The related error statistics are also presented in Table 7.

The high R^2 values (R^2 > 0.95 for all selected wavelengths) and small RMSE values (0.00015 < RMSE < 0.00035) for all the quality-

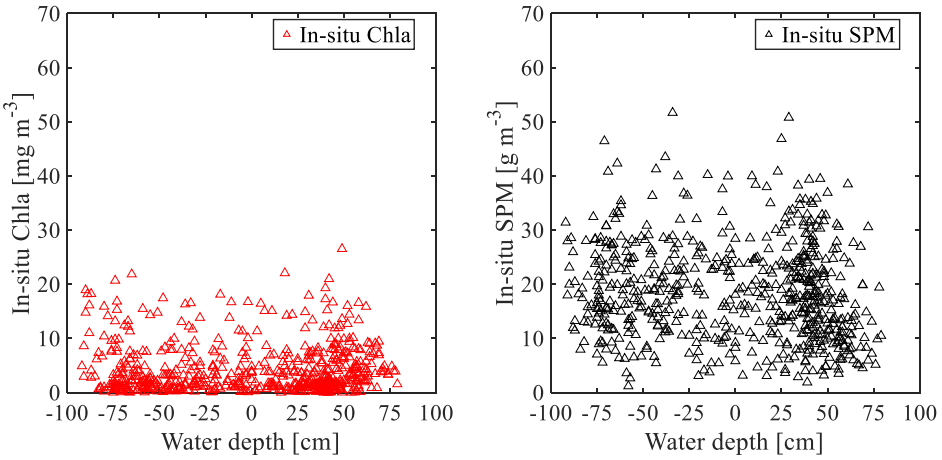

Fig. 11. Left: scatter plot of in-situ Chla concentrations [mg m^{-3}] at the NJS versus water depth values [cm] at the Den Helder station for the quality-controlled dataset between 2008 and 2010; right: the same, for in-situ SPM concentrations [g m^{-3}].

Table 10
The calculated correlation between in-situ Chla [mg m^{-3}] and SPM [g m^{-3}] concentration values between 2008 and 2010 at the NJS and their water depth values [cm] corresponding to different SZA groups.

SZAs/water constituents	Chla [mg m^{-3}]	SPM [g m^{-3}]
[30°–37.5°)	−0.02	−0.12
[37.5°–45°)	−0.34	−0.41
[45°–52.5°)	−0.14	−0.30
[52.5°–60°)	0.09	−0.01
[60°–67.5°)	0.03	0.07
[67.5°–75°]	−0.01	−0.04

Table 11
The mean values of retrieved Chla and SPM concentrations for the flood and ebb groups corresponding to their SZA degrees for the quality-controlled dataset between 2008 and 2010 at the NJS.

SZA/water constituent	Chla [mg m^{-3}]		SPM [g m^{-3}]	
	Flood	Ebb	Flood	Ebb
[30°–37.5°)	7.02	7.10	17.25	19.15
[37.5°–45°)	9.77	8.66	17.66	20.61
[45°–52.5°)	9.93	8.78	20.39	22.86
[52.5°–60°)	8.10	7.93	24.60	26.01
[60°–75°]	4.87	4.97	25.94	28.86

controlled datasets show that the 2SeaColor model is capable of accurately reproducing the measured reflectance spectra for varying WCC values at the NJS. The accuracy of the 2SeaColor model for retrieving Chla and SPM concentrations for the NJS dataset with and without winter retrievals are also illustrated in Figs. 9 and 10, respectively.

Fig. 9 presents the results of the 2SeaColor model validation for retrieving Chla concentrations from a time-series of daily quality-controlled R_{rs} measurements for three years at the NJS. As the Fig. 9 left shows, the model is less successful in achieving reasonable retrievals in winter under high SZAs. However, by removal of the winter retrievals, the retrieved-measured Chla scatter plot shows significant improvement (Fig. 9 right). The related error statistics are also presented in Table 8.

As Table 8 presents, the calculated R^2 and RMSE values of the Chla estimates slightly improve (R^2 from 0.79 to 0.80; RMSE: from 2.57 to 2.98) when the winter retrievals are removed. However, for both groups (with and without winter data), the statistical measures still indicate a reasonable agreement between the retrieved and in-situ Chla concentrations for three years at the NJS.

Fig. 10 also presents the results of the 2SeaColor model validation for retrieving SPM concentrations from a time-series of daily quality-controlled R_{rs} measurements for three years at the NJS. As Fig. 10 left shows, retrievals are less successful in winter under high SZAs. However, by removal of the winter retrievals, the retrieved-measured SPM scatter plot shows improvement (Fig. 10 right). The related error statistics are also presented in Table 9.

As Table 9 shows, the calculated R^2 and RMSE values of the SPM estimates improve significantly when the winter retrievals are removed. Indeed the model shows much better performance to retrieve SPM concentrations after removing the winter retrievals (R^2 = 0.89, RMSE = 2.57 [g m^{-3}]). However, as explained before in Section 5.3, it is uncertain whether this model's deterioration in winter is due to the seasonal pattern of SPM concentrations or due to the SZA effect. Moreover, the accuracy of the 2SeaColor model to retrieve SPM concentration is, as expected, (Salama et al., 2011; Salama and Stein, 2009), better than that for Chla after removal of winter retrievals. The R^2 values are 0.89 and 0.80 and the RMSE values are 2.98 and 2.53 for retrieved Chla and SPM estimates, respectively.

5.5. Tidal effect

To investigate the possible correlation between WCC variations and the tidal cycles over the year at the NJS, the two figures that were produced in Section 5.2 to present the time series (Fig. 4: Chla concentrations versus water depth values, Fig. 5: SPM concentrations versus water depth values) can be used. These figures show the temporal variation of the in-situ Chla and SPM concentrations (black dots) in comparison with their water depth values (grey bars), respectively. As these figures show, no temporal relationship can be found to prove that the concentration of Chla and SPM values at the NJS are affected by the level of water depth. The scatter plots of in-situ Chla and SPM concentrations at the NJS and their corresponding water depth values at the Den Helder station are also presented in Fig. 11.

As can be seen from these figures, no relationships are found between in-situ Chla and SPM concentrations and their corresponding water depth values. The calculated correlation estimates between time series of in-situ Chla and SPM concentrations at the NJS corresponding to their water depth values at the Den Helder station at different SZA groups are also presented in Table 10.

As shown in this table, there are no explicit relationships between measured measurements (i.e. Chla and SPM) and their corresponding water depth values. Table 11 presents the mean values of retrieved Chla and SPM concentrations by the 2SeaColor model during the flood and ebb tide for different SZA groups between 2008 and 2010.

As Table 11 shows, there is no large difference between the mean values of retrieved Chla and SPM concentrations under the conditions of flood and ebb for different SZAs, since the mean differences are < 1.15 [mg m^{-3}] and < 3 [g m^{-3}] for Chla and SPM, respectively, for all groups. Only for SPM, we found that the mean values at flood tend to be slightly lower, which might be due to the inflow of relatively clear water from the North Sea.

6. Discussion

In-situ hyperspectral measurements recorded from fixed offshore platforms can be a cost-effective solution to provide continuous observations for long-term water quality monitoring (Zibordi et al., 2009, 2006). In this study, the two-stream radiative hydro-optical modeling 2SeaColor was applied for the simultaneous retrieval of Chla, SPM and CDOM absorption from a time-series of in-situ R_{rs} measurements recorded between 2008 and 2018 at the NJS located at the Dutch Wadden Sea. Based on the results of this study, the 2SeaColor model shows a good performance in modeling water leaving reflectance spectra (Table 7) and retrieving Chla and SPM concentration values (Tables 8 and 9) using the implemented parameterization in this work (Table 2). The trends of retrieved Chla and SPM values (Figs. 4 and 5) show higher values of Chla (between 10 and 35 [g m^{-3}]) in spring and lower ones in winter (between 0 and 5 [mg m^{-3}]), as well as low values of SPM in spring and summer (between 5 and 30 [g m^{-3}]), and higher values (between 10 and 60 [g m^{-3}]) in winter. These results are in agreement with previous studies for the long-term monitoring of Chla and SPM concentration variations during cruise measurements in the Dutch Wadden Sea (Hommersom, 2010; Hommersom et al., 2009). Furthermore, the performed analysis in the present study revealed that the accuracy of the model deteriorates during winter when the SZA effect and seasonal pattern of WCCs play a role in the quality of in-situ R_{rs} measurements, affecting thereby the accuracy of the retrievals. The results of this study have significant implications for the assessment of the causes and the consequences of long-term water constituent concentrations dynamics in the complex turbid waters of the Dutch Wadden Sea using ground-based measurements and satellite images as follows:

6.1. The implication for water quality monitoring using ground-based measurements

The tidal effect evaluation of this study shows that the NJS is located at a favorable location at the Dutch Wadden Sea, where tides do not significantly influence WCCs (Table 10). This conclusion helps to investigate the monthly, seasonal and annual variation of WCCs retrieved by the 2SeaColor model from time series of in-situ R_{rs} measurements at the NJS, without concerns about the tidal effect on the variation of these WCCs. Otherwise, the studying of the temporal course would become very complicated. In other words, it is fortunate that tidal effects were small, since otherwise we could hardly follow the seasonal courses. Once a hydro-optical model is considered sufficiently valid for WCC retrievals, its temporal predictions can be used for the long-term water quality monitoring at the Dutch Wadden Sea. The validated 2SeaColor model was applied to every 15 min of in-situ R_{rs} measurements collected for more than one decade (from 2002 till present) at the NJS for the simultaneous retrieval of WCCs. These long-term retrievals can later be used to conduct the phenological analysis of Chla concentration and investigation of SPM variation at this area. Of particular interest when conducting Chla phenological analysis, is whether any significant decreasing trend from 2002 until present might indicate the influence of prior nutrient reduction management actions. This has remarkable applications for identifying positive anomaly occurrences and may operate as a warning for water management actions (Arabi et al., 2016). In addition, considering the fair accuracy of the 2SeaColor model (Tables 8 and 9), these accurate long-term observational baselines of SPM and Chla can be used as an indicator to check the accuracy of retrieved WCCs using other water retrieval algorithms in the complex Dutch Wadden Sea.

6.2. The implementation of long-term water quality monitoring using satellite observations

Using a hyperspectral optical model like 2SeaColor, which has been validated under different conditions, and coupling its output to an atmospheric Radiative Transfer (RT) model like MODTRAN following Arabi et al. (2016), allows generating Top Of Atmosphere (TOA) radiance signals for any hyperspectral or multispectral sensor, thus creating a flexible solution that can be applied with any given optical sensor system. The modeled TOA radiance data can next be used in an optimization loop to retrieve all relevant WCCs. Then we will be able to produce retrieved WCCs using satellite images of the Dutch Wadden Sea. Regarding the atmospheric correction, two approaches can be followed: either the atmospheric parameters (aerosol type and visibility) for the whole image are estimated first and next applied to the whole image, or the atmospheric correction parameters are retrieved pixel by pixel, along with the WCCs, in which case the spatial variation of atmospheric properties is accommodated (Arabi et al., 2016; Shen and Verhoef, 2010). At present, there is a full archive of MERIS images of the Dutch Wadden Sea which have been captured from 2002 to 2012. In addition, there is free access to OLCI Sentinel-3 images of the Dutch Wadden Sea since February 2016 (Harvey et al., 2014). Therefore, producing WCC maps retrieved from time series of MERIS (from 2002 to 2012) and OLCI (2016 till present) images will be the next objective of this research. These maps can be used as baseline data for the long-term spatio-temporal monitoring of the area. However, due to the shallowness of large parts of the Dutch Wadden Sea, considering the bottom effect into the hydro-optical retrieval model to produce more reliable WCC maps from satellite images is recommended for these further studies.

7. Conclusion

From the performed analysis and evaluation of this study, we conclude that: (1) the 2SeaColor model is accurate enough to retrieve the concentrations of Chla and SPM during spring and summer for a period of three years (from 2008 to 2010) at the NJS located in the Dutch part of the Wadden Sea; (2) the 2SeaColor model's retrievals of Chla and SPM deteriorate in winter. For Chla, the levels of Chla during winter are too low to be well detectable, and for SPM the concentrations in winter are higher than in the rest of the year. It is therefore uncertain whether the worse results during winter are caused by the seasonal pattern of the concentrations, or by a SZA effect; (3) the SIOPs measured by Hommersom et al. (2009) were found valid for the retrieval of Chla and SPM concentrations. However, measuring seasonally varying SIOPs is recommended for further studies; (4) At the NJS the tide has little observable effects on the diurnal changes of SPM concentration.

Acknowledgment

We thank the Royal Netherlands Institute for Sea Research (NIOZ) for providing the dataset of this research. This work was supported by ITC faculty foundation (ref: IFP17.1.3), University of Twente, the Netherlands.

References

Arabi, B., Salama, M.S., Wernand, M.R., Verhoef, W., 2016. MOD2SEA: a coupled atmosphere-hydro-optical model for the retrieval of chlorophyll-a from remote sensing observations in complex turbid waters. Remote Sens. http://dx.doi.org/10.3390/rs8090722.

Arnone, R., Babin, M., Barnard, A.H., Boss, E., Cannizzaro, J.P., Carder, K.L., Chen, F.R., Devred, E., Doerffer, R., Du, K., Hoge, F., Kopelevich, O.V., Platt, T., Poteau, A.,

Roesler, C., Sathyendranath, S., 2006. Reports of the international ocean-colour coordinating group remote sensing of inherent optical properties: fundamentals, tests of algorithms, and applications. In: IOCCG Report 5, http://dx.doi.org/10.1006/jmbi.1998.2073.

Babin, M., 2003. Variations in the light absorption coefficients of phytoplankton, nonalgal particles, and dissolved organic matter in coastal waters around Europe. Geophys. Res. 108, 2006–2007. http://dx.doi.org/10.1029/2001JC000882.

Babin, M., Morel, A., Fournier-Sicre, V., Fell, F., Stramski, D., 2003. Light scattering properties of marine particles in coastal and open ocean waters as related to the particle mass concentration. Limnol. Oceanogr. 48, 843–859. http://dx.doi.org/10.4319/lo.2003.48.2.0843.

Bashir, Z., 2016. Modeling the Influence of Biological Activity on Fine Sediment Transport in the Dutch Wadden Sea. Mater thesis. Deltares and University of Twente, pp. 1–95. https://www.utwente.nl/en/et/wem/education/msc-thesis/2016/bashir.pdf.

Bricaud, A., Morel, A., Prieur, L., 1981. Absorption by dissolved organic matter of the sea (yellow substance) in the UV and visible domains. Limnol. Oceanogr. 26, 43–53. http://dx.doi.org/10.4319/lo.1981.26.1.0043.

Cadee, G.C., Hegeman, J., 2002. Phytoplankton in the Marsdiep at the end of the 20th century; 30 years monitoring biomass, primary production, and Phaeocystis blooms. J. Sea Res. 48, 97–110. http://dx.doi.org/10.1016/S1385-1101(02)00161-2.

Chaves, J.E., Werdell, P.J., Proctor, C.W., Neeley, A.R., Freeman, S.A., Thomas, C.S., Hooker, S.B., 2015. Assessment of ocean color data records from MODIS-Aqua in the western Arctic Ocean. Deep-Sea Res. II Top. Stud. Oceanogr. 118, 32–43. http://dx.doi.org/10.1016/j.dsr2.2015.02.011.

Chen, X., 2017. Assessment of Satellite-Based Chlorophyll-a Retrieval Algorithms for High Solar Zenith Angle Conditions 11. http://dx.doi.org/10.1117/1.JRS.11.012004.

Doxaran, D., Froidefond, J.M., Castaing, P., Babin, M., 2009a. Dynamics of the turbidity maximum zone in a macrotidal estuary (the Gironde, France): observations from field and MODIS satellite data. Estuar. Coast. Shelf Sci. 81, 321–332. http://dx.doi.org/10.1016/j.ecss.2008.11.013.

Doxaran, D., Ruddick, K., McKee, D., Gentili, B., Tailliez, D., Chami, M., Babin, M., Reintegration, E., Spatiales, C.N. d'Etudes, Programme, B.S.P.O.S.-2, 2009b. Spectral variations of light scattering by marine particles in coastal waters, from visible to near infrared. 54, 1257–1271. http://dx.doi.org/10.4319/lo.2009.54.4.1257.

Duntley, S.Q., 1941. The optical properties of diffusing materials. J. Opt. Soc. Am. 61–70. http://dx.doi.org/10.1364/JOSA.32.000061.

Eleveld, M.A., Van der Wal, D., Van Kessel, T., 2014. Estuarine suspended particulate matter concentrations from sun-synchronous satellite remote sensing: tidal and meteorological effects and biases. Remote Sens. Environ. 143, 204–215. http://dx.doi.org/10.1016/j.rse.2013.12.019.

Fettweis, M., Nechad, B., Van den Eynde, D., 2007. An estimate of the suspended particulate matter (SPM) transport in the southern North Sea using SeaWiFS images, in situ measurements and numerical model results. Cont. Shelf Res. 27, 1568–1583. http://dx.doi.org/10.1016/j.csr.2007.01.017.

Gordon, H.R., Brown, O.B., Evans, R.H., Brown, J.W., Smith, R.C., Baker, K.S., Clark, D.K., 1988. A semianalytic radiance model of ocean color. J. Geophys. Res. Atmos. 93, 10909–10924. http://dx.doi.org/10.1029/JD093iD09p10909.

Gupta, H.V., Kling, H., Yilmaz, K.K., Martinez, G.F., 2009. Decomposition of the mean squared error and NSE performance criteria: implications for improving hydrological modelling. J. Hydrol. 377, 80–91. http://dx.doi.org/10.1016/j.jhydrol.2009.08.003.

Harvey, E.T., Kratzer, S., Philipson, P., 2014. Satellite-based water quality monitoring for improved spatial and temporal retrieval of chlorophyll-a in coastal waters. Remote Sens. Environ. 158, 417–430. http://dx.doi.org/10.1016/j.rse.2014.11.017.

He, X., Bai, Y., Pan, D., Huang, N., Dong, X., Chen, J., Chen, C.A., Cui, Q., 2013. Using geostationary satellite ocean color data to map the diurnal dynamics of suspended particulate matter in coastal waters. Remote Sens. Environ. 133, 225–239. http://dx.doi.org/10.1016/j.rse.2013.01.023.

Hommersom, A., 2010. Modeling the Influence of Biological Activity on Fine Sediment Transport in the Dutch Wadden Sea. http://hdl.handle.net/1871/15939.

Hommersom, A., Peters, S., Wernand, M.R., de Boer, J., 2009. Spatial and temporal variability in bio-optical properties of the Wadden Sea. Estuar. Coast. Shelf Sci. 83, 360–370. http://dx.doi.org/10.1016/j.ecss.2009.03.042.

Hommersom, A., Peters, S.W.M., Van Der Woerd, H.J., Eleveld, M.A., Wernand, M.R., de Boer, J., 2010. Tracing Wadden Sea water masses with an inverse bio-optical and endmember model. EARSeL e-Proceedings 9, 1–12.

IOCCG, 2000. Remote sensing of ocean colour in coastal, and other optically-complex, waters. In: Reports of the International Ocean-Colour Coordinating Group, No. 3. IOCCG, Dartmouth, Canada. http://www.ioccg.org/reports/report3.pdf.

Kirk, J.T.O., 1994. Light and photosynthesis in aquatic ecosystems. J. Mar. Biol. Assoc. U. K. 74, 987. http://dx.doi.org/10.1017/S0025315400044180.

Lee, Z., Carder, K.L., Mobley, C.D., Steward, R.G., Patch, J.S., 1998. Hyperspectral remote sensing for shallow waters. I. A semianalytical model. Appl. Opt. 37, 6329–6338. http://dx.doi.org/10.1364/AO.37.006329.

Lee, Z., Carder, K.L., Mobley, C.D., Steward, R.G., Patch, J.S., 1999. Hyperspectral remote sensing for shallow waters. 2. Deriving bottom depths and water properties by optimization. Appl. Opt. 38, 3831–3843. http://dx.doi.org/10.1364/AO.38.003831.

Lee, Z., Carder, K.L., Arnone, R.A., 2002. Deriving inherent optical properties from water color: a multiband quasi-analytical algorithm for optically deep waters. Appl. Opt. 41, 5755–5772. http://dx.doi.org/10.1364/AO.41.005755.

Li, H., He, X., Bai, Y., Chen, X., Gong, F., Zhu, Q., Hu, Z., 2017. Assessment of satellite-based chlorophyll-a retrieval algorithms for high solar zenith angle conditions. J. Appl. Remote. Sens. 11, 12004. http://dx.doi.org/10.1117/1.JRS.11.012004.

Loisel, H., Vantrepotte, V., Jamet, C., Dat, D.N., 2013. Challenges and new advances in ocean color remote sensing of coastal waters. Oceanogr. Res. 1–38. http://dx.doi.org/10.5772/56414.

Mélin, F., Vantrepotte, V., Clerici, M., D'Alimonte, D., Zibordi, G., Berthon, Canuti, E., 2011. Multi-sensor satellite time series of optical properties and chlorophyll-a concentration in the Adriatic Sea. Prog. Oceanogr. 91, 229–244. http://dx.doi.org/10.1016/j.pocean.2010.12.001.

Mobley, C.D., 1994. Light and Water: Radiative Transfer in Natural Waters. Academic Press. http://www.jstor.org/stable/26231610.

Mobley, C.D., Gentili, B., Gordon, H.R., Jin, Z., Kattawar, G.W., Morel, A., Reinersman, P., Stamnes, K., Stavn, R.H., 1993. Comparison of numerical models for computing underwater light fields. Appl. Opt. http://dx.doi.org/10.1364/AO.32.007484.

Morel, A., Maritorena, S., 2001. Bio-optical properties of oceanic waters: a reappraisal. Geophys. Res. 106, 7163–7180. http://dx.doi.org/10.1029/2000JC000319.

Niedermeier, A., Hoja, D., Lehner, S., 2005. Topography and morphodynamics in the German bight using SAR and optical remote sensing data. Ocean Dyn. 55, 100–109. https://link.springer.com/article/10.1007%2Fs10236-005-0114-2.

Petzold, T., 1972. Volume Scattering Functions for Selected Ocean Waters. Scripps Inst. Ocean. SIO Ref., pp. 72–78. http://www.dtic.mil/dtic/tr/fulltext/u2/753474.pdf.

Philippart, C.J.M., Van Iperen, J.M., Cadee, G.C., Zuur, A.F., 2010. Long-term field observations on seasonality in chlorophyll-a concentrations in a shallow coastal marine ecosystem, the Wadden Sea. Estuar. Coasts 33, 286–294. http://dx.doi.org/10.1007/s12237-009-9236-y.

Philippart, C.J.M., Salama, M.S., Kromkamp, J.C., Van Der Woerd, H.J., Zuur, A.F., Cadée, G.C., 2013. Four decades of variability in turbidity in the western Wadden Sea as derived from corrected Secchi disk readings. Sea Res. 82, 67–79. http://dx.doi.org/10.1016/j.seares.2012.07.005.

Pope, R.M., Fry, E.S., 1997. Absorption spectrum (380-700 nm) of pure water. II. Integrating cavity measurements. Appl. Opt. 36, 8710–8723. http://dx.doi.org/10.1364/AO.36.008710.

Ridderinkhof, H., Zimmerman, J.T.F., Philippart, M.E., 1990. Tidal exchange between the North Sea and Dutch Wadden Sea and mixing time scales of the tidal basins. Neth. J. Sea Res. 25, 331–350. http://dx.doi.org/10.1016/0077-7579(90)90042-F.

Salama, M.S., Shen, F., 2010. Stochastic inversion of ocean color data using the cross-entropy method. Opt. Express 18, 479–499. http://dx.doi.org/10.1364/OE.18.000479.

Salama, M.S., Stein, A., 2009. Error decomposition and estimation of inherent optical properties. Appl. Opt. 48, 4947–4962. http://dx.doi.org/10.1364/AO.48.004947.

Salama, M.S., Su, Z., 2010. Bayesian model for matching the radiometric measurements of aerospace and field ocean color sensors. Sensors 10, 7561–7575. http://dx.doi.org/10.3390/s100807561.

Salama, M.S., Verhoef, W., 2015. Two-stream remote sensing model for water quality mapping: 2SeaColor. Remote Sens. Environ. 157, 111–122. http://dx.doi.org/10.1016/j.rse.2014.07.022.

Salama, M.S., Monbaliu, J., Coppin, P., 2004. Atmospheric correction of advanced very high resolution radiometer imagery. Remote Sens. 25, 1349–1355. http://dx.doi.org/10.1080/01431160310001592283.

Salama, M.S., Mélin, F., Van Der Velde, R., 2011. Ensemble uncertainty of inherent optical properties. Opt. Express 304, 16772–16783. http://dx.doi.org/10.1364/OE.19.016772.

Salama, M.S., Radwan, M., van der Velde, R., 2012. A hydro-optical model for deriving water quality variables from satellite images (HydroSat): a case study of the Nile River demonstrating the future Sentinel-2 capabilities. Phys. Chem. Earth 50–52, 224–232. http://dx.doi.org/10.1016/j.pce.2012.08.013.

Shen, F., Verhoef, W., 2010. Suppression of local haze variations in MERIS images over turbid coastal waters for retrieval of suspended sediment concentration. Opt. Express 18, 12653–12662. http://dx.doi.org/10.1364/OE.18.012653.

Sijtsma, F.J., Broersma, L., Daams, M.N., Hoekstra, H., Werner, G., 2015. Tourism development in the Dutch Wadden area: spatial-temporal characteristics and monitoring needs. Environ. Manag. Sustain. Dev. 4, 217. http://dx.doi.org/10.5296/emsd.v4i2.8561.

Valente, A.S., da Silva, J.C.B., 2009. On the observability of the fortnightly cycle of the Tagus estuary turbid plume using MODIS Ocean colour images. J. Mar. Syst. 75, 131–137. http://dx.doi.org/10.1016/j.jmarsys.2008.08.008.

Van der Woerd, H.J., Pasterkamp, R., 2008. HYDROPT: a fast and flexible method to retrieve chlorophyll-a from multispectral satellite observations of optically complex coastal waters. Remote Sens. Environ. 112, 1795–1807. http://dx.doi.org/10.1016/j.rse.2007.09.001.

Volpe, G., Santoleri, R., Vellucci, V., d'Alcalà, M.R., Marullo, S., D'Ortenzio, F., 2007. The colour of the Mediterranean Sea: global versus regional bio-optical algorithms evaluation and implication for satellite chlorophyll estimates. Remote Sens. Environ. 107, 625–638. http://dx.doi.org/10.1016/j.rse.2006.10.017.

Wang, Y., 1997. Satellite SAR Imagery for Topographic Mapping of the Tidal Flat Areas in the Dutch Wadden Sea. PhD thesis. 172 Fac. Soc. Behav. Sci.. http://hdl.handle.net/11245/1.134894.

Wang, M., 2007. Remote sensing of the ocean contributions from ultraviolet to near-infrared using the shortwave infrared bands: simulations. Appl. Opt. 46, 1535–1547. http://dx.doi.org/10.1364/AO.46.001535.

Wang, M., Bailey, S.W., 2001. Correction of sun glint contamination on the SeaWiFS ocean and atmosphere products. Appl. Opt. 40, 4790. http://dx.doi.org/10.1364/AO.40.004790.

Wang, M., Gordon, H.R., 1994. A simple, moderately accurate, atmospheric correction algorithm for SeaWiFS. Remote Sens. Environ. 50, 231–239. http://dx.doi.org/10.1016/0034-4257(94)90073-6.

Wang, M., Shi, W., 2007. The NIR-SWIR combined atmospheric correction approach for MODIS ocean color data processing. Opt. Express 15, 15722–15733. http://dx.doi.org/10.1364/OE.15.015722.

Wang, M., Tang, J., Shi, W., 2007. MODIS-derived ocean color products along the China east coastal region. Geophys. Res. Lett. 34, 1–5. http://dx.doi.org/10.1029/

2006GL028599.
Wang, M., Son, S., Shi, W., 2009. Evaluation of MODIS SWIR and NIR-SWIR atmospheric correction algorithms using SeaBASS data. Remote Sens. Environ. 113, 635–644. http://dx.doi.org/10.1016/j.rse.2008.11.005.
Wang, M., Ahn, J.-H., Jiang, L., Shi, W., Son, S., Park, Y.-J., Ryu, J.-H., 2013. Ocean color products from the Korean Geostationary Ocean Color Imager (GOCI). Opt. Express 21, 3835–3849. http://dx.doi.org/10.1364/OE.21.003835.
Wernand, M.R., 2002. Guidelines for (Ship-Borne) Auto-Monitoring of Coastal and Ocean Colour. Ocean Optics. http://melia.nioz.nl/phptoweb/colors/documentation/colours38.htm.
Wernand, M.R., 2011. Historical Archives of Ocean Colour in Global - Change Perspective. Ph.D. Thesis. Univ. Utrecht, Netherlands. https://dspace.library.uu.nl/handle/1874/212589.
Wernand, M.R., van Der Woerd, H.J., 2010. Ocean colour changes in the North Pacific since 1930. J. Eur. Opt. Soc. Rapid Publ. 5, 10015s. http://dx.doi.org/10.2971/jeos.2010.10015s.
Wimmer, C., Siegmund, R., Schwabisch, M., Moreira, J., 2000. Generation of high precision DEMs of the Wadden Sea with airborne interferometric SAR. IEEE Trans. Geosci. Remote Sens. 38, 2234–2245. http://dx.doi.org/10.1109/36.868881.
Yu, X., Salama, M.S., Shen, F., Verhoef, W., 2016a. Retrieval of the diffuse attenuation coefficient from GOCI images using the 2SeaColor model: a case study in the Yangtze Estuary. Remote Sens. Environ. 175, 109–119. http://dx.doi.org/10.1016/j.rse.2015.12.053.
Yu, X., Shen, F., Liu, Y., 2016b. Light absorption properties of CDOM in the Changjiang (Yangtze) estuarine and coastal waters: an alternative approach for DOC estimation. Estuar. Coast. Shelf Sci. 181, 302–311. http://dx.doi.org/10.1016/j.ecss.2016.09.004.
Zibordi, G., Strömbeck, N., Mélin, F., Berthon, J.F., 2006. Tower-based radiometric observations at a coastal site in the Baltic proper. Estuar. Coast. Shelf Sci. 69, 649–654. http://dx.doi.org/10.1016/j.ecss.2006.05.022.
Zibordi, G., Berthon, J.F., Mélin, F., D'Alimonte, D., Kaitala, S., 2009. Validation of satellite ocean color primary products at optically complex coastal sites: northern Adriatic Sea, northern Baltic proper and gulf of Finland. Remote Sens. Environ. 113, 2574–2591. http://dx.doi.org/10.1016/j.rse.2009.07.013.